NASA TECHNICAL MEMORANDUM

NASA TM X-53076

JUNE 25, 1964

NASA TM X-53076

PRECISION OPTICAL TRACKING SYSTEM FOR ADVANCED LAUNCH VEHICLES

by CHARLES L. WYMAN, KLAUS JUERGENSEN, ROBERT L. KURTZ, LARRY HAYES, AND JOHN M. GOULD
Astrionics Laboratory

NASA

George C. Marshall Space Flight Center, Huntsville, Alabama

TECHNICAL MEMORANDUM X-53076

PRECISION OPTICAL TRACKING SYSTEM FOR ADVANCED LAUNCH VEHICLES

By

Charles L. Wyman, Klaus Juergensen, Robert L. Kurtz,
Larry Hayes, and John M. Gould

George C. Marshall Space Flight Center
Huntsville, Alabama

ABSTRACT

The development efforts on an experimental optical radar system for precision tracking for advanced launch vehicles during the early launch phase are described. Basic concepts for a prototype system are discussed along with some advanced techniques that are being investigated. Analyses and investigations concerning the project are discussed. An error analysis is made assuming a tracker that measures elevation angle, azimuth angle, and distance in digital form. The analysis is concerned with errors in distance, velocity, and acceleration computed from distance measurements. The distance measurements are assumed to be inaccurate by a systematic error and a distributed error. Also, the error caused by linear interpolation between displayed points is considered. No data smoothing is taken into account. Equations are developed that can be used to obtain optimal data rate and highest frequency with which the true range and angular parameters may change without causing errors exceeding the required accuracies.

A trajectory analysis is performed utilizing a typical Saturn V trajectory to determine the dynamic range of the instrument parameters. Vehicle and instrument parameters are plotted against time, and the curves are used for design purposes.

A range analysis develops optical radar equations. The system uses retrodirective corner reflectors on the booster to increase the return signal. The increase is calculated and included in the range equations along with calculations of atmospheric attenuation. A preliminary calculation of background radiation is made.

A preliminary synthesis of the tracking mount servo assumes a type one servo with tachometer stabilization. The analysis indicates that the system has the desired static accuracy in the presence of high breakaway friction, can operate at very small dynamic errors, and exhibits good stability.

An investigation concerning refractive and turbulence effects of the atmosphere on laser beams is discussed.

NASA-GEORGE C. MARSHALL SPACE FLIGHT CENTER

NASA-GEORGE C. MARSHALL SPACE FLIGHT CENTER

TECHNICAL MEMORANDUM X-53076

PRECISION OPTICAL TRACKING SYSTEM FOR ADVANCED LAUNCH VEHICLES

By

Charles L. Wyman, Klaus Juergensen, Robert L. Kurtz,
Larry Hayes, and John M. Gould

APPLIED RESEARCH BRANCH
ASTRIONICS LABORATORY
RESEARCH AND DEVELOPMENT OPERATIONS

TABLE OF CONTENTS

TABLE OF CONTENTS (con't)

LIST OF ILLUSTRATIONS

LIST OF ILLUSTRATIONS (Cont'd)

LIST OF TABLES

TECHNICAL MEMORANDUM X-53076

PRECISION OPTICAL TRACKING SYSTEM FOR ADVANCED LAUNCH VEHICLES

SUMMARY

Precision tracking of space boosters during the first 50 seconds of flight cannot be satisfactorily accomplished by present day techniques. Laser technology has advanced to the point where systems can be designed. An optical radar system using a continuous gas laser can perform the tracking to the required accuracies.

The proposed system will measure distance, angles, velocities, and acceleration in spherical coordinates. An error analysis reveals that:

a. The distance can be computed with the required accuracy if the data rate used for distance computation exceeds a minimal value and if the systematic error of the distance measurement does not exceed a maximal value.

b. Velocity and acceleration can be computed with the required accuracies if the true distance frequency does not exceed a maximal value and if the optimal data rate is used for computation. The formulas for the critical values mentioned above are tabulated in the report.

The range analysis indicates that radar systems using coherent optical wavelengths are characterized by very high antenna gain. The extreme directivity of the laser beam results in elimination of ground clutter, very precise angular information, and a high signal to noise ratio. The servo analysis describes closed loop operation of the tracking system. All pertinent transfer functions are derived, the necessary compensating filters are computed, and the loop is analyzed for stability and accuracy.

SECTION I. INTRODUCTION AND SYSTEM PHILOSOPHY

By

Charles L. Wyman

Present day tracking of space boosters during the early launch phase is unsatisfactory. Real time information is practically nonexistent. Recorded data from radar, photographic, and television tracking systems are marginal at best and do not allow sufficient evaluation of the post-flight trajectory.

Accuracy requirements as determined by flight evaluation personnel are specified in Table I. Satisfaction of the Class III requirements is the object of this development. Tracking accuracies of present day systems, for the first 50 seconds of flight, rarely satisfy Class I position requirements. Velocity and acceleration data are even less satisfactory.

Satisfaction of the Class III tracking requirements allows the following evaluations:

a. Establishment of liftoff motion.

b. Evaluation of vehicle dynamics and malfunctions.

c. Evaluation of guidance and propulsion system performance.

d. Determination of dynamic pressure to less than 1 percent.

The feasibility of using coherent optical sources for extremely accurate tracking has already been established by previous studies and experiments (Refs. 1 and 2). This project will result in the development of an experimental prototype tracking system mechanized to allow evaluation of various state-of-the-art measuring techniques. An optimum system will be determined based on the results achieved by the experimental system.

The studies are being performed to determine the parameters and characteristics of the system. Limitations of various techniques and concepts are deduced and the most promising approaches are singled out for further investigation. The various studies are as follows:

a. Error analysis. To enable determination of the precision with which measurements must be made to fulfill the system requirements.

TABLE I

EARLY LAUNCH PHASE TRACKING REQUIREMENTS				
FLIGHT INTERVAL	DATA REQUIRED	REDUCED DATA ACCURACY		
		CLASS I	CLASS II	CLASS III
1. 0 - 5 seconds	position	0.5 m	0.1 m	0.1 m
	velocity	1.0 m/s	0.1 m/s	0.1 m/s
	acceleration	0.2 m/s^2	0.5 m/s^2	0.01 m/s^2
2. 5 - 25 seconds	position	5.0 m	1.0 m	1.0 m
	velocity	1.0 m/s	0.1 m/s	0.1 m/s
	acceleration	0.5 m/s^2	0.1 m/s^2	0.02 m/s^2
3. 25 - 50 seconds	position	30 m	10 m	5 m
	velocity	1.0 m/s	0.2 m/s	0.1 m/s
	acceleration	0.5 m/s^2	0.1 m/s^2	0.02 m/s^2

b. Trajectory analysis. To determine various trajectory parameters with respect to the tracking site.

c. Range analysis. To evaluate source and detector characteristics.

d. Analysis of refractive and turbulence effects of the atmosphere. To determine the magnitude of these sources of error and the basic system limitation.

e. Servo analysis and synthesis. To determine the specifications of equipment for the experimental system and to gain insight as to the nature of the tracking problem.

Nomenclature

θ	half power beam angle of a receiver aperture
λ	carrier wavelength
d	diameter of receiver aperture
$\delta\lambda$	range resolution
E	signal power
N	noise power
f_d	doppler shifted difference frequency
V	velocity

A. DESCRIPTION OF BASIC SYSTEM

Range measurement with radar systems presents no great problem (Ref. 3). With multiple-frequency, continuous-wave radar systems, range can typically be measured to a small fraction of the shortest wavelength being monitored.

However, angle measurement presents another problem. The angular resolution of microwave systems is usually about 1/10 the diffraction limited angle of the antenna. The diffraction limited angle is

$$\theta \approx \frac{\lambda}{d} \qquad (1)$$

where θ is the angle between half power points of the signal, λ is the signal wavelength, and d is the diameter of the receiver antenna. Typically, θ is about 0.1 to 1 degree for microwave radar. Optical elements are also diffraction limited. The angular accuracy of optical systems is limited by the pointing accuracy of the pedestal.

With this increased angular resolution, much better position accuracy is possible than with other types of systems.

The system being developed is a single station range and angle measuring device using a modulated beam from a gas laser operating at a visible wavelength. Figure 1 is an artist's conception of the system. The narrow light beam from the laser is reflected off an array of optical corner reflectors located on the Saturn vehicle. Range and angle are measured with reference to the corner reflectors. The various functions are described below:

1. Angular error information is derived from the return signal by an image dissector photomultiplier used with a 15 cm diameter receiving telescope. The instantaneous field of view is about 30 arc seconds, and an angle can be measured to a small fraction of this. The angular position of the tracking mount is measured with 19-bit digital shaft encoders. Overall angular accuracy of the basic system is expected to be about 5 arc seconds.

2. Range is determined by measuring the phase shift between the transmitted and the received beams at the modulation frequencies. Three frequency operations are contemplated at approximately 30 kHz, 1 MHz, and 30 MHz. The 30 kHz operation allows coarse range measurement to 10 km without encountering ambiguous readings. This coarse range can be measured to an accuracy determined by

$$\delta\lambda_{(30\ \mathrm{kHz})} = \frac{\lambda_{(30\ \mathrm{kHz})}}{2\pi\,(2\ \mathrm{E/N})^{\frac{1}{2}}} \qquad (2)$$

where the numerator is the wavelength at the given frequency and E/N is the signal to noise ratio. A signal to noise ratio of 50 gives a range accuracy of

$$\delta\lambda_{(30\ \mathrm{kHz})} = \frac{10^4}{6.28 \times 10} \approx 160\ \mathrm{m}. \qquad (3)$$

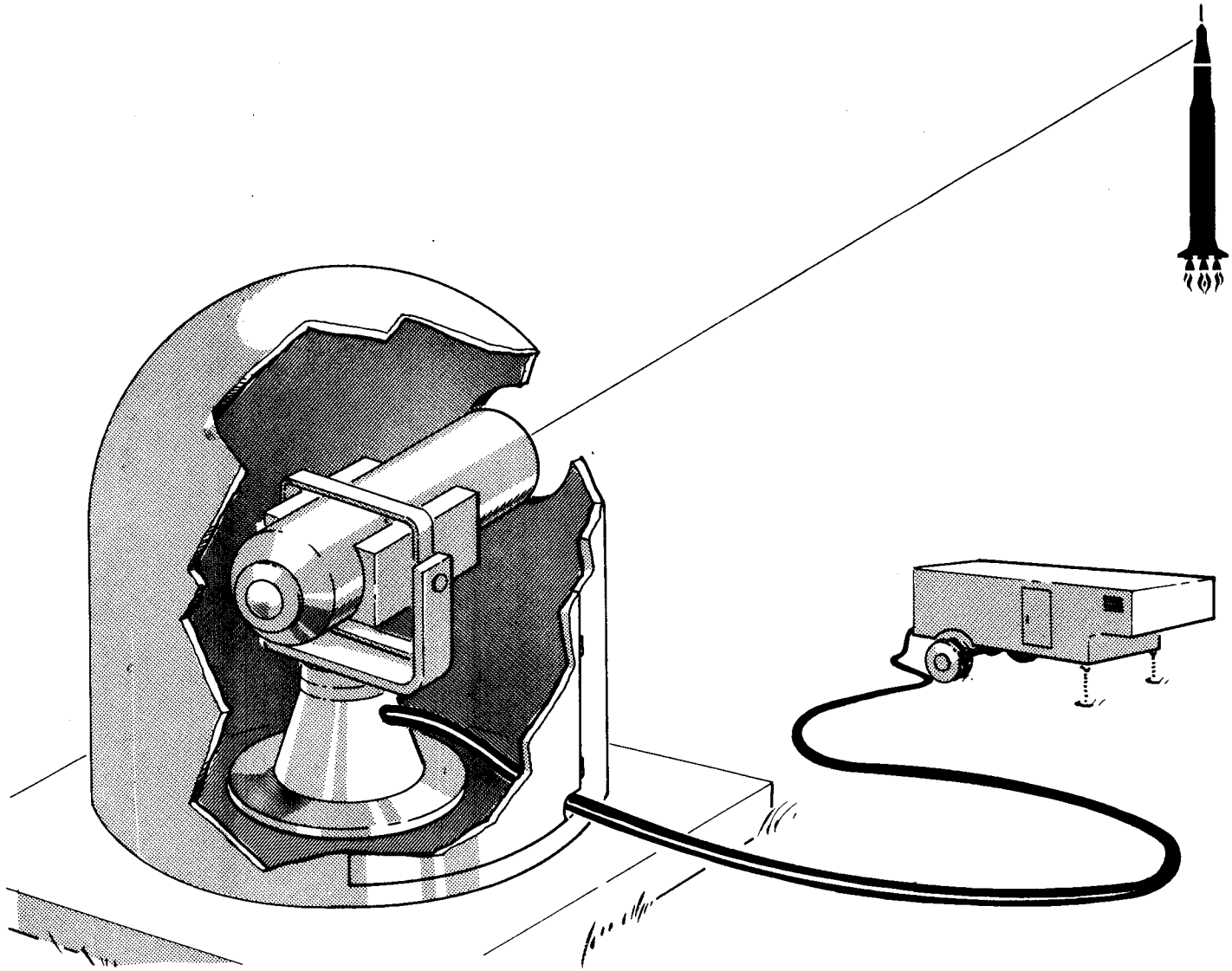

Figure 1. Optical Radar System.

Following the same reasoning using other frequencies, one can see that resolution at 1 MHz is

$$\delta\lambda_{(1.0\ \text{MHz})} = \frac{300}{62.8} \approx 3.8\ \text{m}. \tag{4}$$

Resolution at 30 MHz is

$$\delta\lambda_{(30\ \text{MHz})} = \frac{10}{62.8} \approx 0.16\ \text{m}. \tag{5}$$

A higher signal to noise ratio results in better range resolution.

A photomultiplier will be used for detection of the range signal. Beam splitting optics, used with the receiving telescope, channel part of the received energy to the range detector and part to the angle detector. Multilayer dielectric filters will be used to reduce background light.

3. Position of the vehicle is calculated from the range and angle measurements. Velocity and acceleration are calculated from successive differentiations of position data. Smoothing and averaging are necessary to obtain the required accuracy of acceleration from the position data.

4. A narrow-angle acquisition system is being contemplated which utilizes an electro-optical beam steering device to scan a field of approximately one degree.

With this technique, a portion of the transmitter beam will be deflected in azimuth and elevation by 100 times the beam width. A beam width of 30 arc seconds divergence is planned. A raster scan similar to that of television systems will be used. As the beam is scanned across the corner reflectors on the vehicle, a pulse of light will be returned to the receiver. An acquisition detector with the appropriate field of view detects the pulse which is time-correlated with the raster scan to locate the target. The requirements for a wide angle acquisition system have not been determined.

B. ADVANCED TECHNIQUES

The basic system as described has two major drawbacks. First, the two axis tracking pedestal is a state-of-the-art design. It must be maintained

in a temperature stable environment to avoid angular errors caused by thermal stresses and distortions. Second, while the expected position accuracies will fulfill Class III requirements, the first and second derivatives yield marginal velocity information and unsatisfactory acceleration data. However, the accuracy of this system will far surpass systems based on radio frequency and photographic techniques. Furthermore, unlike photographic systems, the information will be in real time.

The drawbacks might be alleviated by certain advanced measuring techniques. Therefore, it is desirable to investigate the feasibility and practicality of various concepts. Such concepts could be applied toward an optimum system. Following are techniques and concepts under consideration.

1. A three station tracking system that will measure the angle accurately for the first few seconds of the trajectory and thereafter measure the range to alleviate the first difficulty. A further improvement would be to make the transmitter and receiver stationary and to direct the transmitted beam and receiver field of view with a simplified pedestal equipped with a plane mirror. This simplification would result in a tracking pedestal of much smaller size and relaxed environmental requirements. Measurements that can be made with the single station tracking system can be used to define the requirements for a three station system.

2. Optical superheterodyning techniques are under study in two inhouse laboratory investigations. If these techniques prove feasible for use in a tracking system, the second problem could be alleviated. Detection of the doppler shift frequency of the returned beam by these techniques would allow a direct measurement of the line of sight component of vehicle velocity. Less smoothing would be required to determine acceleration to the desired accuracy. The major drawback with this type operation is that the bandwidth requirements are very high. This is easily seen when one realizes that, for every wavelength of the optical carrier that the vehicle moves, two cycles are generated. The doppler-shifted difference frequency is

$$fd = \frac{2v}{\lambda} . \qquad (6)$$

Typical advanced Saturn trajectory data indicate difference frequencies up to 600 MHz during the early launch phase.

3. A third measurement technique that would alleviate both problem areas is being considered. This technique calls for accurate angular rate and acceleration measurements of the tracking pedestal. Recent state-of-the-art developments indicate that both may be practical and inexpensive. Use of the recently developed ring laser system appears to be an excellent way to measure angular rate to extremely high precision (Ref. 4). The ring laser is a completely static device and will not generate any disturbing torques or other forces on the pedestal. Furthermore, the device shows promise of being very small and inexpensive. It appears that eventually the angular drift rates of the device will be low enough to integrate angular rate to determine angular position with greater precision than with shaft encoders. Direct angular rate measurements made with range measurements allow more accurate velocity determination than the basic system. A ring laser system will be evaluated for possible use on the tracking system. Angular acceleration measuring devices are being investigated further.

C. CONCLUSIONS

The basic system being developed will be a versatile research tool allowing experimentation and investigations leading to design data for optimum optical tracking and ranging systems. Furthermore, this basic system will have the capability of actually performing the tracking function to a much greater accuracy than existing systems.

The various investigations being performed in support of this project will be important to many types of electro-optical systems. The superheterodyne experiments and the atmospheric propagation studies will be useful to this project and to all organizations having optical tracking and communication problems.

The studies discussed in this report are those that are most necessary to the definition of the tracking problem and to the determination of the system characteristics. This report will be updated in the future and will include results of the superheterodyne and atmospheric propagation studies along with descriptions and explanations of some of the key subsystems, such as the ring laser and the laser transmitter. Design and development of the optical system are being initiated and will be discussed in a future report.

SECTION II. ERROR ANALYSIS AND FREQUENCY RESPONSE OF OPTICAL TRACKER

By

Klaus Juergensen

The proposed optical tracker will measure the position of the target in spherical coordinates by measuring digitally the azimuth angle, the elevation angle, and the distance. Each of the three outputs is assumed to be erroneous by a statistically distributed error and a systematic error. A computer is proposed to obtain from the angle and distance measurements the angular and linear velocities and accelerations. Possibly, the computer will also convert the data from spherical coordinates into Cartesian coordinates. The latter process is not considered in this study.

The author wishes to acknowledge the contributions of John M. Gould which were essential in the preparation of this study.

Nomenclature

x;y	distance
j	systematic distance error
h	distributed distance error
v;c	velocity
α;b	acceleration
A	amplitude of acceleration
ϵ_x	error in distance
ϵ_y	error in velocity
ϵ_a	error in acceleration

ν_x	minimal data rate for distance
ν_{00}	optimal data rate for velocity
ν_a	data rate for acceleration
ν_0	optimal data rate for acceleration
t	time
2λ	time between two displays of acceleration data
2μ	time between two displays of velocity data
2η	time between two displays of distance data
ω	2π times target distance frequency
ω_0	highest ω with free choice of $\frac{M}{K}$ without exceeding ϵ_a
ω_0*	highest ω with optimal choice of $\frac{M}{K}$ without exceeding ϵ_a
ω_{00}*	highest ω without exceeding ϵ_v
K, M, N	see Figures 4 and 6 for definition

A. INTRODUCTION

Since the problem of obtaining angular velocity and angular acceleration data from angular measurements is exactly the same as that of obtaining linear velocity and linear acceleration from distance measurements, only the formulas for distance, linear velocity, and linear acceleration are developed. The formulas can be used for the azimuth and elevation coordinates by simply replacing distance and distance error with angle and angular error.

The distance data will be displayed every 2η seconds. The distance data between displayed points may be obtained by linear interpolation. The maximal possible* difference between any so obtained distance information and the true distance is considered the distance error (Fig. 2).

*See asterisk on following page.

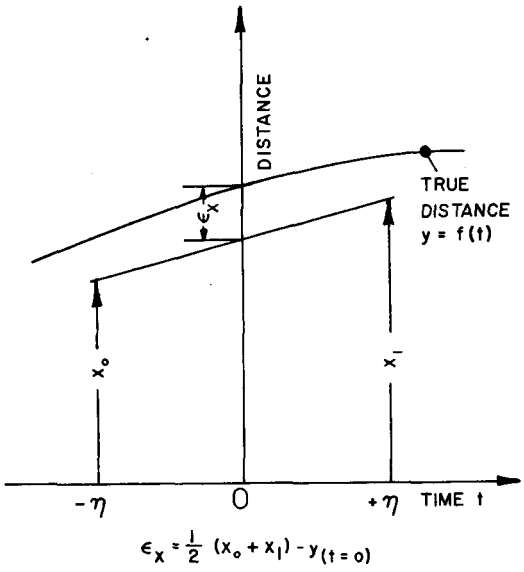

Figure 2. Definition of Error in Distance.

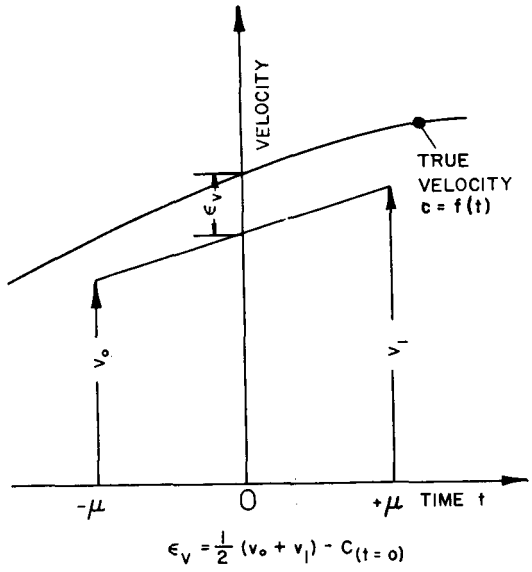

Figure 3. Definition of Error in Velocity.

The velocity data will be displayed every 2μ seconds. The velocity data between displayed points may be obtained by linear interpolation. The maximal possible* difference between any so obtained velocity information and the true velocity is considered the velocity error (Fig. 3). The velocity data are obtained by subtracting two distance measurements at time t and time t + $2N\mu$ and dividing the difference by $2N\mu$ (Fig. 4).

The acceleration data will be displayed every 2λ seconds. The acceleration data between displayed points may be obtained by linear interpolation. The maximal possible* difference between any so obtained acceleration information and the true acceleration is considered the acceleration error (Fig. 5). The acceleration informations α_0 at time t and α_1 at time t + 2λ are obtained by the following process (Fig. 6):

1. By subtracting $X_{40} - X_{30}$ and dividing by $2M\lambda$, the velocity V_{40} is obtained.

---

*For the computation of the maximal possible error in distance, velocity, and acceleration, the 3 σ value of the distributed error in the distance measurements is considered. The more detailed study shows that the maximal possible error occurs in the middle between displayed points when the true curves of distance, velocity, and accleration have extreme values. Therefore, the simple expression for ϵ_a, ϵ_v, and ϵ_x as shown in Figures 2, 3, and 5 are correct.

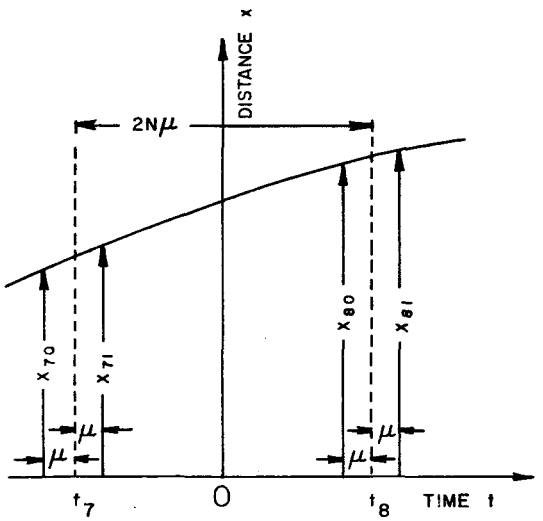

Figure 4. Graphical Representation of Data Processing Leading to Velocity Information.

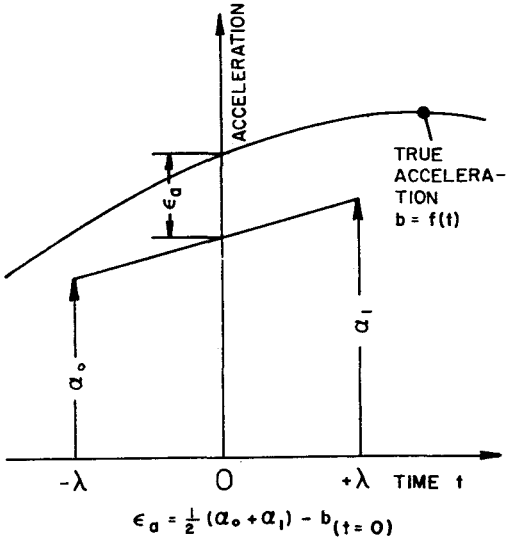

Figure 5. Definition of Error in Acceleration.

2. By subtracting $X_{60} - X_{50}$ and dividing by $2M\lambda$, the velocity V_{60} is obtained.

3. By subtracting $V_{60} - V_{40}$ and dividing by $2K\lambda$, the acceleration α_0 is obtained.

4. By processing the distance data X_{41}, X_{31}, X_{61}, and X_{51} in exactly the same way, the acceleration α_1 is obtained.

Since the thrust of the target vehicle is limited, a maximal possible acceleration is assumed. Furthermore, it is assumed that the true distance changes sinusoidally.

The object of this study is to determine which data rate is required and how fast the true distance may change without causing errors exceeding the required accuracy. No allowance is made for an error caused by the computer because it is assumed that the digital system carries enough digits to make the computational error negligible compared with the errors caused by inaccurate input data. The following is a summary of a more detailed study.

B. ERROR ANALYSIS FOR ACCELERATION

The distance data are measured as shown in Figure 6. Each distance measurement x contains the distributed error h and the systematic error j.

The velocity is obtained by:

$$\text{at } t = t_1 - \lambda: \qquad V_{40} = \frac{X_{40} - X_{30}}{2M\lambda}$$

$$\text{at } t = t_1 + \lambda: \qquad V_{41} = \frac{X_{41} - X_{31}}{2M\lambda}$$

$$\text{at } t = t_2 - \lambda: \qquad V_{60} = \frac{X_{60} - X_{50}}{2M\lambda}$$

$$\text{at } t = t_2 + \lambda: \qquad V_{61} = \frac{X_{61} - X_{51}}{2M\lambda}.$$

The acceleration is obtained by:

$$\text{at } t = -\lambda: \qquad \alpha_0 = \frac{X_{60} - X_{50} - X_{40} + X_{30}}{4\ MK\ \lambda^2}$$

$$\text{at } t = +\lambda: \qquad \alpha_1 = \frac{X_{61} - X_{51} - X_{41} + X_{31}}{4\ MK\ \lambda^2} \qquad \text{(Fig. 5)}$$

The error in acceleration is

$$\epsilon_a = -A \left[1 - \frac{\sin K\omega\lambda \sin M\omega\lambda \cos \omega\lambda}{MK\ \omega^2\ \lambda^2}\right] +$$

$$+ \frac{h_{60} + h_{30} - h_{50} - h_{40} + h_{61} + h_{31} - h_{51} - h_{41}}{8\ MK\ \lambda^2} +$$

$$+ \frac{j_{60} + j_{30} - j_{50} - j_{40} + j_{61} + j_{31} - j_{51} - j_{41}}{8\ MK\ \lambda^2}.$$

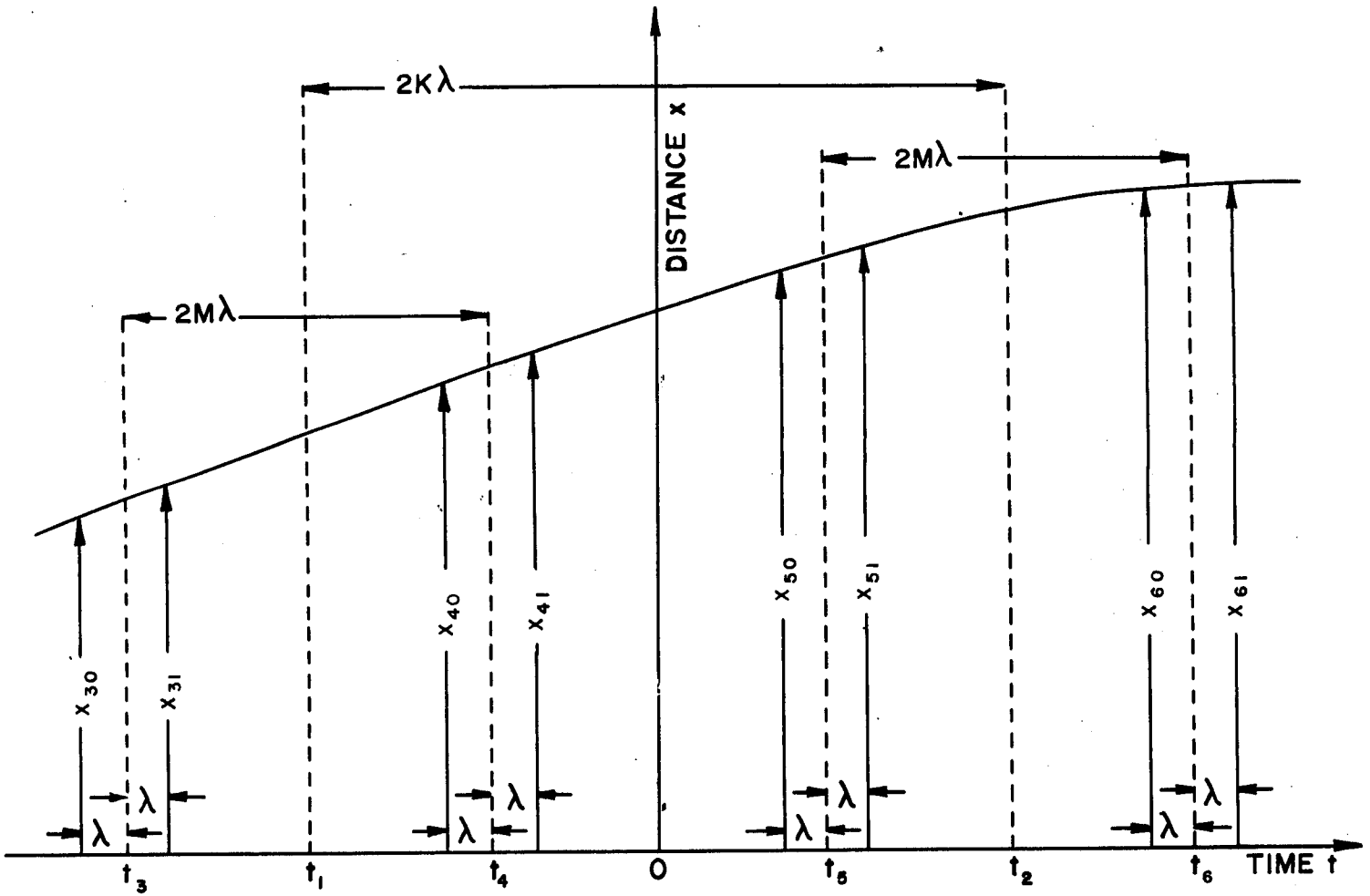

Figure 6. Graphical Representation of Data Processing Leading to Acceleration Information.

If the distributed error h is the same for all eight distance measurements, the second term yields

$$\pm \frac{\sqrt{2}\, h}{4\, MK\, \lambda^2}.$$

If the systematic error j is the same during the time interval from $t = t_3 - \lambda$ to $t = t_6 + \lambda$, the third term cancels. For these cases, error in acceleration yields

$$\epsilon_a = -A \left[1 - \frac{\sin K\omega\lambda \sin M\omega\lambda \cos \omega\lambda}{MK\, \omega^2 \lambda^2}\right] \pm \frac{\sqrt{2}\, h}{4\, MK\, \lambda^2}.$$

Since we are considering small values of $K\omega\lambda$, $M\omega\lambda$, and $\omega\lambda$, the following approximations are used

$$\sin K\omega\lambda \approx K\omega\lambda - \frac{1}{6} (K\omega\lambda)^3$$

$$\sin M\omega\lambda \approx M\omega\lambda - \frac{1}{6} (M\omega\lambda)^3$$

$$\cos \omega\lambda \approx 1 - \frac{1}{2} (\omega\lambda)^2$$

$$\epsilon_a \approx - A\, \lambda^2 \left(\frac{1}{6} K^2 + \frac{1}{6} M^2 + \frac{1}{2}\right) \omega^2 - \frac{\sqrt{2}\, h}{4\, MK\, \lambda^2}.$$

By introducing data rate $\nu_a = \frac{1}{2\lambda}$ and solving the formula for ϵ_a for ω, we obtain

$$\omega \approx \sqrt{\frac{-4\, \epsilon_a}{A \left(\frac{1}{6} K^2 + \frac{1}{6} M^2 + \frac{1}{2}\right)}} \sqrt{\nu_a^2 - \frac{\sqrt{2}\, h}{MK\, \epsilon_a}\, \nu_a^4}.$$

The maximum value of ω_0 of ω for variable rate ν_a and constant values for A, K, M, h, and ϵ_a is obtained at optimal data rate ν_0

$$\nu_0^2 \approx -\frac{MK\,\epsilon_a}{2\sqrt{2}\,h}$$

and will reach the value

$$\omega_0 \approx \epsilon_a \sqrt{\frac{\sqrt{2}}{Ah}} \sqrt{\frac{1}{\frac{1}{MK} + \frac{1}{3}\left(\frac{K}{M} + \frac{M}{K}\right)}} .$$

The highest value for the factor

$$\sqrt{\frac{1}{\frac{1}{MK} + \frac{1}{3}\left(\frac{K}{M} + \frac{M}{K}\right)}} = \sqrt{\frac{3\,M^2}{3 + 2\,M^2}}$$

will be reached if we make K = M. Thus the highest $\omega_0 = \omega_0^*$ will be

$$\omega_0^* \approx \epsilon_a \sqrt{\frac{\sqrt{2}}{A\,h}} \sqrt{\frac{3\,M^2}{3 + 2\,M^2}}$$

with optimal data rate $\nu_0^2 \approx -\frac{M^2\,\epsilon_a}{2\sqrt{2}\,h}$ and K = M.

The formula for ω_0^* clearly shows that M should be made as high as possible to obtain high ω_0^*. However, ν_0 becomes high at the same time which is inconvenient. Table II shows how the normalized ω_0^* ($\omega_0^* = 1$ for $M = \infty$) and the normalized ν_0 ($\nu_0 = 1$ for M = 1) change with M. Table II also shows that to keep ν_0 down, one should choose M to be between 3 and 5. This means a sacrifice in ω_0^* of about 10 percent of the best obtainable ω_0^* at $M = \infty$.

TABLE II

OPTIMAL DATA RATE FOR ACCELERATION

M	ω_0*	ν_0	
∞	1	∞	
10	0.988	10	
5	0.943	5	reasonable compromise
4	0.916	4	
3	0.858	3	
2	0.727	2	
1	0.400	1	

C. ERROR ANALYSIS FOR VELOCITY

The same considerations as in the previous section are applied. The distance data are measured as shown in Figure 4. Each distance measurement x contains the distributed error h and the systematic error j. The velocity is obtained by

$$\text{at } t = -\mu: \qquad V_0 = \frac{X_{80} - X_{70}}{2N\mu}$$

$$\text{at } t = +\mu: \qquad V_1 = \frac{X_{81} - X_{71}}{2N\mu} \qquad \text{(Fig. 3)}.$$

Assuming h to be the same for all four distance measurements and j to be constant during the time interval from $t = t_7 - \mu$ to $t_8 + \mu$, the velocity error is

$$\epsilon_v = \frac{A}{\omega}\left(1 - \frac{\sin \omega N\mu \cos \omega\mu}{\omega N\mu}\right) \pm \frac{h}{2N\mu}.$$

By the same considerations previously discussed, the highest frequency for which we can hold the velocity error ϵ_v is

$$\omega_{00}^* \approx \frac{32}{27} \frac{\epsilon_v^3}{A h^2} \frac{3N^2}{3 + N^2}$$

which requires an optimal data rate ν_{00} of

$$\nu_{00} \approx \frac{2}{3} \frac{N \epsilon_v}{h}.$$

D. ERROR ANALYSIS FOR DISTANCE

The previous considerations are applied for the error analysis for distance. The calculations show that a systematic error j (which is assumed to be constant for the time of $\Delta t = 2\eta$) does not cancel. Since the computations are based on a maximal possible amplitude A in acceleration, very low frequencies create the biggest errors. The error is

$$\epsilon_x = A \eta^2 \frac{1 - \cos \omega\eta}{\omega^2 \eta^2} \pm \frac{\sqrt{2}}{2} h + j$$

where

$$0 \leqq \frac{1 - \cos \omega\eta}{\omega^2 \eta^2} \leqq \frac{1}{2} \qquad \text{for all } \omega.$$

To stay within the error limit $\pm \epsilon_x$, η must be

$$\eta \leqq \sqrt{\frac{2}{A} \left(\epsilon_x - \frac{\sqrt{2}}{2} h - j \right)}$$

or

$$\nu_x = \frac{1}{2\eta} \geqq \frac{1}{2} \sqrt{\frac{A}{2 \left(\epsilon_x - \frac{\sqrt{2}}{2} h - j \right)}}.$$

The limit of systematic error j is

$$|j| \leqq \epsilon_x - \frac{\sqrt{2}}{2} h.$$

E. COMPILATION OF FORMULAS AND NUMERICAL VALUES

1. Distance:

Limit for j:

$$|j| \leqq \epsilon_x - \frac{\sqrt{2}}{2}\, h$$

Minimum data rate:

$$\nu_x = \frac{1}{2} \sqrt{\frac{A}{2\left(\epsilon_x - \frac{\sqrt{2}}{2}\, h - j\right)}}$$

2. Velocity:

Optimal data rate:

$$\nu_{00} \approx \frac{2}{3}\, \frac{N\, \epsilon_v}{h}$$

Maximal ω:

$$\omega_{00}^* \approx \frac{32}{27}\, \frac{\epsilon_v^3}{A\, h^2}\, \frac{3\, N^2}{3+N^2}$$

3. Acceleration:

Optimal data rate:

$$\nu_0 \approx \sqrt{-\frac{M^2\, \epsilon_a}{2\sqrt{2}\, h}}$$

Maximal ω:

$$\omega_0^* \approx \epsilon_a \sqrt{\frac{\sqrt{2}}{Ah}}\, \sqrt{\frac{3\, M^2}{3 + 2M^2}}$$

Assumed values used in numerical computations are

ϵ_a	$= \pm 0.01$ m/s^2	$\lvert j_{max} \rvert$	$= 0.029$ m
ϵ_v	$= \pm 0.1$ m/s	ν_x	$= 6.53$ Hz
ϵ_x	$= \pm 0.1$ m	ν_{00}	$= 3.33$ Hz
h	$= \pm 0.1$ m	ω_{00}^*	$= 0.0317$ rad/s
N	$= 5$	ν_0	$= 0.94$ Hz
M	$= 5$	ω_0^*	$= 0.142$ rad/s
A	$= \pm 10$ m/s^2		
j	$= 0$ m		

SECTION III. TRAJECTORY ANALYSIS OF THE EARLY LAUNCH PHASE TRACKER

By

Robert Lee Kurtz

A. INTRODUCTION

An optical tracking system to track the Saturn V for the first 60 seconds of flight is being developed. The tracking system will be located some distance from the launch site and will measure slant range, radial velocity, and azimuth and elevation angles. For design purposes, it is necessary to determine the dynamic range of these and other instrument parameters.

A typical Saturn V trajectory is analyzed to determine the range of some of these parameters for a specific location of the instrument relative to the launch site. The trajectory information was taken from a computer readout. The vehicle ground range and altitude, relative to the launch site, are used to calculate the instrument parameters. The vehicle and instrument parameters are plotted against time.

Nomenclature

ρ	instrument slant range
ρ'	instrument ground range
I	instrument
m	vehicle
θ	azimuth angle
φ	elevation angle
$\overline{\omega}$	average angular velocity
$\overline{\alpha}$	average angular acceleration
x_m	measured ground range (vehicle system)

y_m	measured altitude (vehicle system)
z_m	separation of coordinate system = 1 kilometer
Δy	approximation altitude error
H	corrected altitude (flat earth)
c_x	chord length = corrected range (flat earth)
s	arc length = true range (XXXE system)
E_r	true altitude (XXXE system)
r	radius of the earth (constant in XXXE system)
Δx	approximation range error
ℓ	general value of perpendicular distance from polar plane to earth surface
A	projected value of r in the vertical plane

B. DESCRIPTION OF COORDINATE SYSTEM

A procedure for parameter transformation from a vehicle coordinate system to an optical tracking instrument coordinate system has been analyzed. Values of vehicle range and altitude were obtained from a typical Saturn V trajectory readout. The values used in this analysis are referenced to an earth-fixed coordinate (XXXE) system. The XXXE system allows the altitude to be measured from the surface of a constant radius earth, positive up along a plumb-line which describes the y axis. The range in the XXXE system is measured along the periphery of the constant radius earth. The value of this constant radius for the earth is 6,373,384.1 meters, which is the value for a Florida launch point determined by the Clark Reference Ellipsoid. The values of vehicle range and altitude in this XXXE system for the present investigation were considered as the standard or true values and all measurement values were compared to them.

Parameter transformation from vehicle to instrument coordinate system was effected since data on vehicle position parameters were readily available in the form of typical values of a Saturn V firing. Using these values of range and

altitude from the XXXE system and transformation equations from the instrument coordinate system, the variation of such instrument parameters as φ, θ, ρ, and ρ' was found.

The problem is to choose a suitable coordinate reference system for the optical tracking instrument and to determine typical maximum and minimum values of the instrument parameters through the use of a typical trajectory readout of the Saturn V vehicle system.

For the present analysis, the following conditions will be imposed. These conditions, however, have not been determined to be optimum for the system.

Conditions:

1. The origin of the instrument coordinate system will be located on the positive z axis, 1 km from the origin of the vehicle coordinate system.

2. The vehicle travel will be considered to remain always in the plane of the firing azimuth, i.e., the xy plane of the vehicle coordinate system (Fig. 7).

3. A "flat earth" will be considered for reasons of geometrical simplicity, and the approximation errors resulting from the geometry of this consideration will be calculated.

4. From the typical Saturn V readout, the earth-referenced position parameters of the XXXE system was used. This earth-referenced system allows the altitude to be measured from the surface of the earth perpendicularly up along a plumbline called the y axis. Range is measured along the periphery of a constant radius earth.

5. Through the use of typical Saturn V firing readout values of range and altitude and the equations of transformation, typical values of instrument parameters will be obtained.

Using the flat earth considerations mentioned previously, vehicle position, velocity, and acceleration parameters will be referenced to an orthogonal Cartesian coordinate system, shown in Figure 7. Altitude of the vehicle will be measured perpendicular to the xz plane up along the positive y axis. The value of this variable displacement will be called y_m. Ground range of the vehicle, because of this flat earth concept, will be measured from the origin of the Cartesian coordinate system along the positive x axis. The value of this variable displacement along the x axis will be called x_m. For this analysis, the vehicle

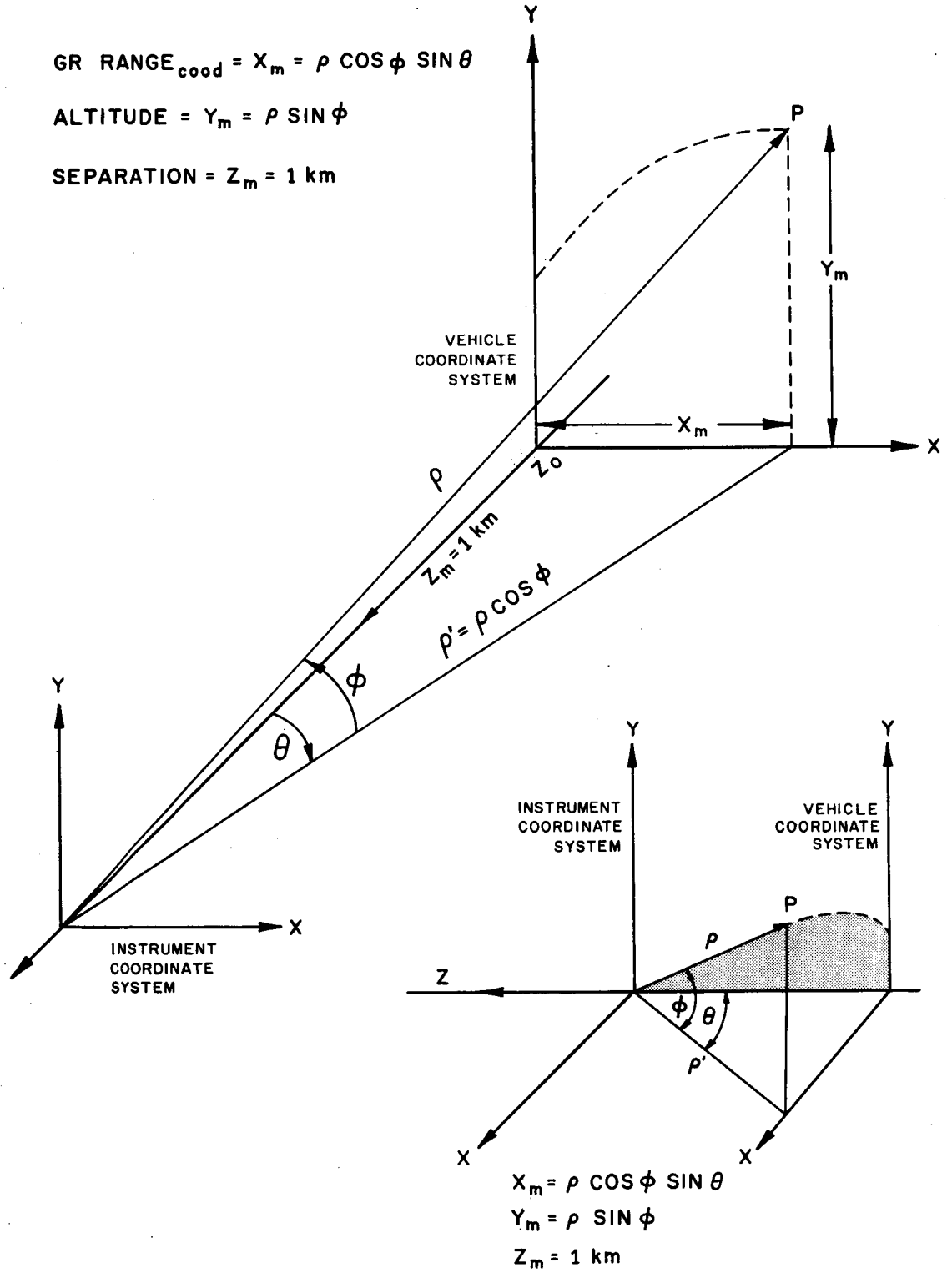

Figure 7. Coordinate System Relations.

travel will always be confined to the xy plane, i.e., no roll or yaw will be considered. This Cartesian coordinate system for the measurement of vehicle parameters is a right-handed system and the positive direction of the z axis is as indicated in Figure 7. The coordinate system used to reference the optical tracking instrument parameters has its origin on the positive z axis of the vehicle Cartesian coordinate system. The origin of the instrument coordinate system is displaced one kilometer from the origin of the vehicle coordinate system along the positive direction of the z axis. Therefore, the distance of separation of the two coordinate systems is a constant one kilometer and will be called z_m.

The optical tracking instrument will use a standard spherical coordinate system, modified so that its azimuthal angle θ and elevation angle φ may be zero referenced to the positive z axis of the vehicle system described above. The positive direction of azimuthal angle θ is from the xz plane up along the direction of the positive y axis. Positive increase of the elevation angle φ produces positive values of y_m. The positive direction of the angles θ and φ is indicated by the arrowheads in Figure 7.

The transformation equations giving the relations between the coordinates of the vehicle rectangular coordinate system and the instrument modified spherical coordinate system are as follows:

$$x_m = \rho \cos \varphi \sin \theta \tag{1}$$

$$y_m = \rho \sin \varphi \tag{2}$$

$$z_m = 1 \text{ km}. \tag{3}$$

where ρ is the instrument slant range and the line of sight from the origin of the instrument coordinate system to the vehicle.

From Figure 7, we see that the azimuthal angle is

$$\theta = \tan^{-1} \frac{x_m}{z_m}, \tag{4}$$

and the elevation angle is

$$\varphi = \tan^{-1} y_m/\rho' = \tan^{-1} \frac{y_m \cos \theta}{z_m} \tag{5}$$

since ρ' is the projection of ρ onto the xz plane and is equal to $z_m/\cos \theta$.

Again, from flat earth considerations, the ground range x_m will be measured along the positive direction of the x axis of the vehicle coordinate system and in the xz plane. The altitude y_m will be measured along the positive direction of the y axis of the vehicle coordinate system and in the xy plane. These flat earth measurements of ground range x_m and altitude y_m constitute an approximation to the XXXE system values of ground range s and altitude E_r. Since the XXXE system is to be considered our standard, differences will exist between the measured values (flat earth) and the standard (XXXE). These differences produce approximation errors. From the geometry of the situation, equations will be derived for these approximation errors and their magnitudes will be calculated.

C. TREATMENT OF SYSTEM PARAMETERS

The typical Saturn V firing readout furnishes values of vehicle ground range and altitude every 0.25 seconds. These values from the XXXE system are considered the standard or true values for this analysis. Ground range s and altitude E_r in this XXXE system are earth-referenced as indicated earlier.

Because of the geometry, values of vehicle ground range and altitude x_m and y_m, respectively, as measured by the optical tracking instrument, will not be exactly equal to the XXXE reference or true values. The degree of approximation of the true values by the measured values is high when one considers the magnitude of the approximation errors, which will be calculated later.

The values of vehicle ground range and altitude from the typical Saturn V readout are depicted in Figures 8 and 9, respectively. When these values are

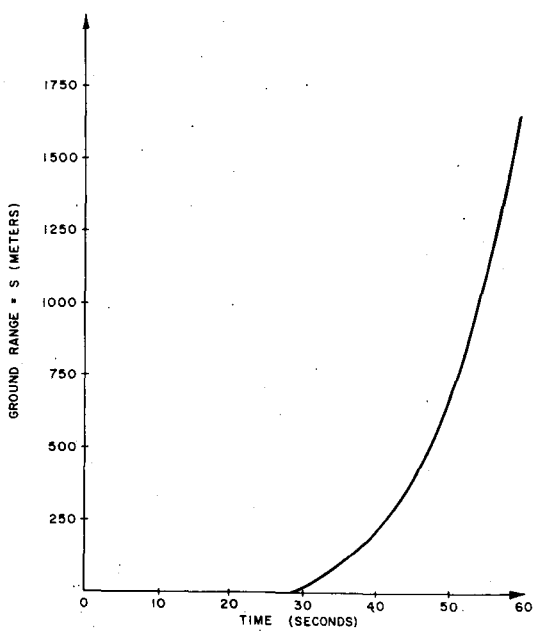

Figure 8. Range Versus Time.

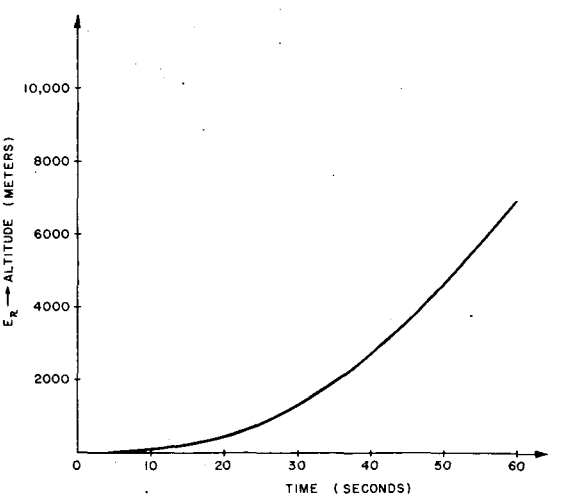

Figure 9. Altitude Versus Time.

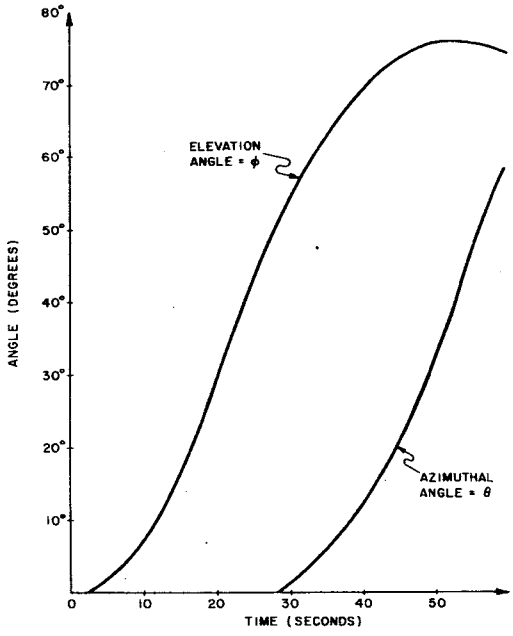

Figure 10. Elevation and Azimuthal Angles, θ and φ, Versus Time.

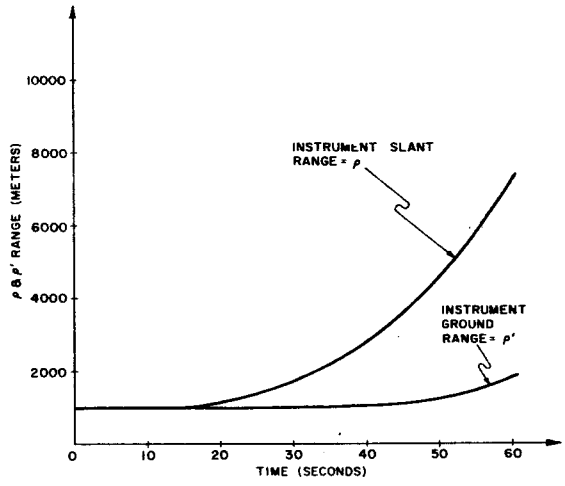

Figure 11. Instrument Slant and Ground Range Versus Time.

substituted into the equations of transformation, one can find the typical variation of such instrument parameters as

θ = Azimuthal angle

φ = Elevation angle

ρ = Instrument slant range

ρ' = Instrument ground range.

The variation of azimuthal angle θ and elevation angle φ is illustrated in Figure 10. This is the case where the separation of the instrument coordinate system is one kilometer from the origin of the vehicle coordinate system. An increase in this distance of separation will result typically in a corresponding decrease in the magnitude of angles θ and φ.

Knowing the magnitude variation of the angles θ and φ with time and using the equations of transformation, one can find the range of variation of instrument slant range and instrument ground range ρ and ρ', respectively. The variation of these with time, up to 60 seconds, is depicted in Figure 11.

Having determined the value of elevation angle φ and azimuthal angle θ at 0.25 second time intervals, the average angular velocities may be calculated from the following equations:

Average angular elevation velocity,

$$\overline{\omega}_{\varphi} = \frac{\varphi_2 - \varphi_1}{t_2 - t_1} = \frac{\Delta\varphi}{\Delta t}. \tag{6}$$

Average angular azimuthal velocity,

$$\overline{\omega}_{\theta} = \frac{\theta_2 - \theta_1}{t_2 - t_1} = \frac{\Delta\theta}{\Delta t}. \tag{7}$$

Since the graphs are intended to represent trend only, it was expedient to take velocity averages over a time interval of three seconds. These velocity variations over a period of 60 seconds are given in Figure 12.

From the calculated angular velocities, the average angular accelerations were found with the aid of the following equations:

Average angular acceleration of φ

$$\overline{\alpha}_{\varphi} = \frac{\overline{\omega}_{\varphi_2} - \overline{\omega}_{\varphi_1}}{t_2 - t_1} = \frac{\Delta\overline{\omega}_{\varphi}}{\Delta t}. \tag{8}$$

Average angular acceleration of θ,

$$\overline{\alpha}_{\theta} = \frac{\overline{\omega}_{\theta_2} - \overline{\omega}_{\theta_1}}{t_2 - t_1} = \frac{\Delta\overline{\omega}_{\theta}}{\Delta t}. \tag{9}$$

The trend of these accelerations, taken over a three-second time interval, is depicted in Figure 13.

In this treatment of system parameters, the approach has been to take typical standard values of range and altitude from the XXXE system and, with the aid of the transformation equations, to derive the typical range of variation of instrument parameters such as θ, φ, ρ, and ρ'.

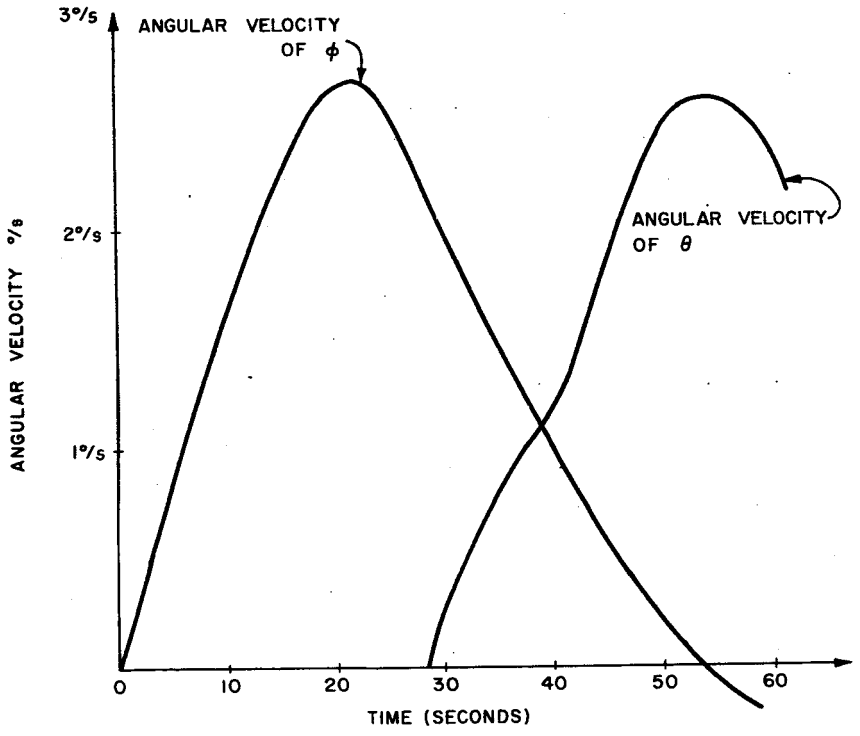

Figure 12. Angular Velocity of φ and θ Versus Time.

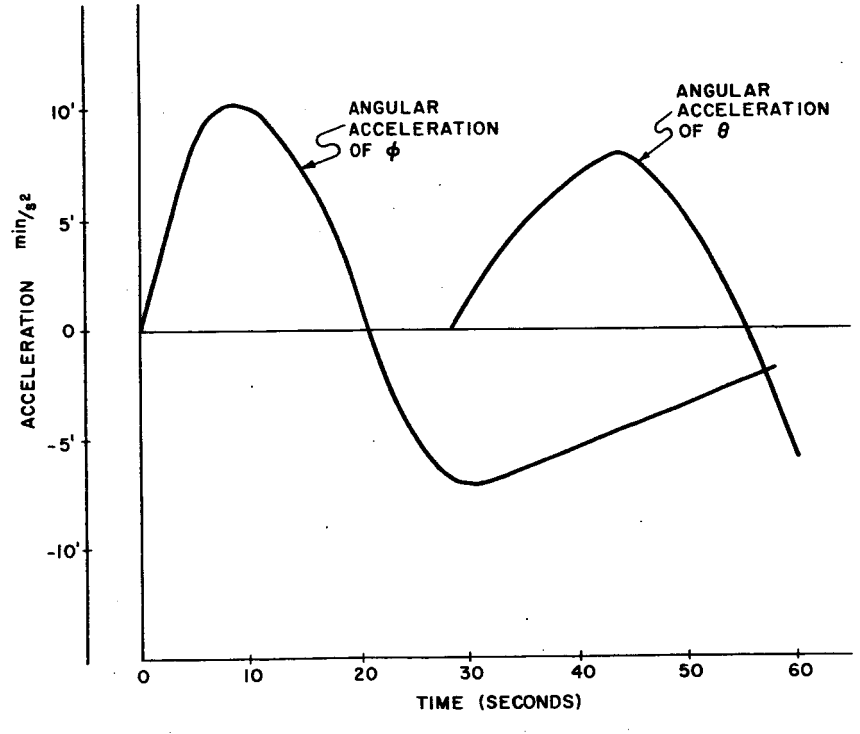

Figure 13. Angular Acceleration of φ and θ Versus Time.

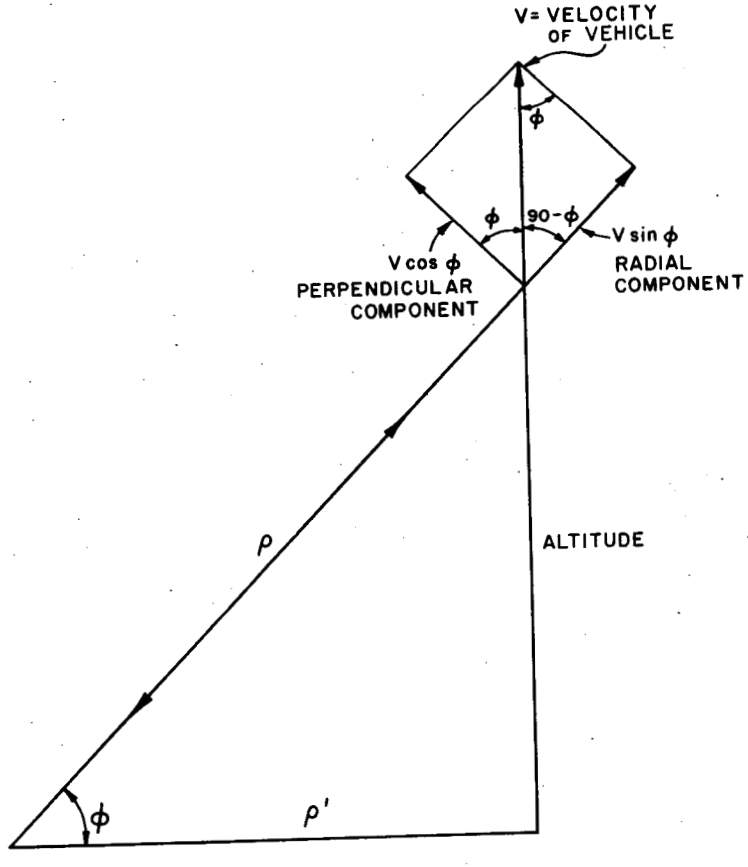

Figure 14. Special Case - Doppler Effect.

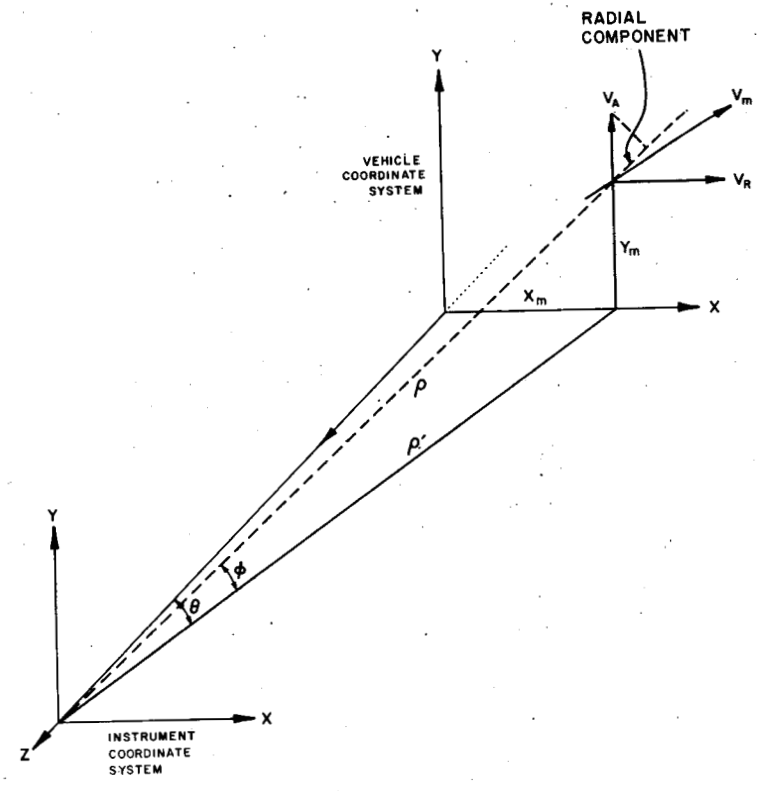

Figure 15. General Case - Doppler Effect.

The range and range rate will be obtained from the doppler effect. Figure 14 depicts the case of doppler effect where transmission is in the plane of the vehicle. Assume that a transmitted ray travels along the distance and direction of ρ and is incident on a retrodirective reflector on board a vehicle which travels vertically upward. Only the radial component of vehicle velocity along the line of sight, i.e., in the direction of the ray, will cause a doppler shift on the returned beam.

The more practical case for measurement of doppler shift is shown in Figure 15. There are two primary differences between this case and the one discussed previously. First, the transmitted ray makes some angle with the plane of the vehicle; i.e., the transmitter is displaced some distance z from the plane of the vehicle and "looks" at the vehicle from an angle. Secondly, the vehicle velocity vector makes some angle with the vertical. The details of this case will be treated in a later report.

D. APPROXIMATIONS CAUSED BY "FLAT EARTH" CONSIDERATIONS

The values of vehicle ground range x_m and altitude y_m measured with reference to the flat plane by the optical tracking instrument are only approximations to the true or standard values of vehicle ground range s and altitude E_r in the XXXE system which is referenced to the constant radius earth. The magnitude of the approximation errors must be determined and the relation between these and the measured values of range and altitude x_m and y_m, respectively, must be known if the measured x_m and y_m are to produce an acceptable approximation of range and altitude.

The equations relating the approximations and approximation errors are derived and a summary table of approximation parameters is given to show specific relations of these terms.

As pointed out earlier, extreme simplification of the geometrical problem results when a flat earth approximate condition is used and measured parameters are all referenced to a flat plane tangent to the earth at the point of launch. In this case, the elevation and azimuthal angles φ and θ, respectively, will always be acute angles of their respective right triangles.

Figure 16 shows the flat earth plane, which is the xz plane of the vehicle• coordinate system. The vehicle ground range x_m as measured with the optical tracking instrument will be measured in this plane along the positive direction of

the x axis. The altitude y_m measured by the optical instrument will be measured from this flat earth plane perpendicularly up along the positive y axis of the vehicle coordinate system.

Again from Figure 16, the ground range of the XXXE system or the standard being used is measured along an arc of the constant radius earth. This range taken over an arc of the constant radius earth was previously designated as s. The altitude of the XXXE system, previously designated as E_r, is measured from the surface of the constant radius earth perpendicularly up to the target, along a positive extension of the earth's radius.

From the geometry of the flat-earth/round-earth approximation relations, Figure 16, and the situation description above, it is seen that:

1. The chord length c_x along the positive x axis approximates the true range s measured along the arc length. The relation between the measured range x_m and the value c_x is

$$c_x = x_m - \Delta x \tag{10}$$

where c_x is the corrected range parameter that acceptably approximates the true range s. Therefore, the range approximation error is Δx.

2. The perpendicular distance H, measured from the point H_0 in Figure 16 up along the positive y axis, approximates the true altitude E_r measured from the earth's surface up along a positive extension of the earth radius. The relation between the measured altitude y_m and the value H is

$$H = y_m + \Delta y \tag{11}$$

where H is the corrected altitude parameter which acceptably approximates the true altitude E_r. Therefore, the altitude approximation error is Δy.

Now from the geometry of Figure 16 and the equations 10 and 11, the magnitude of the range and altitude approximation errors Δx and Δy, respectively, will be calculated. The value of these approximation errors will be calculated after 60 seconds of flight time. This will determine a maximum value for the error since the error increases with the angles φ and θ, and these angles are maximum at about 60 seconds of flight time.

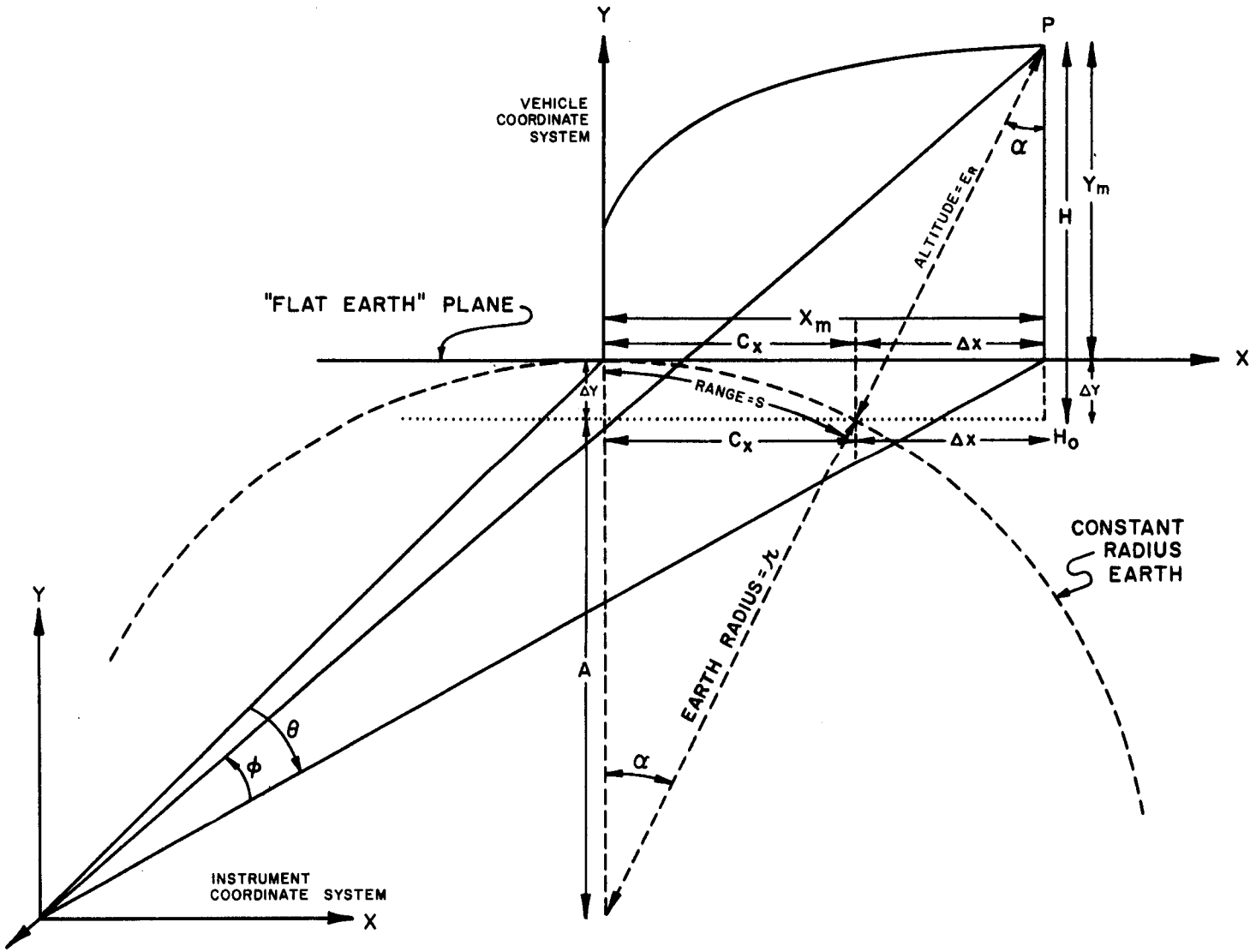

Figure 16. Flat-Earth/Round-Earth Approximation Relations.

The value of the central angle α between displacements of the earth's radius will now be computed (Fig. 16). From the relation

$$\alpha = s/r \tag{12}$$

where

s = arc length = range in XXXE system

r = constant radius of earth,

note that

$$\alpha = \frac{1632.2952 \text{ m}}{6373384.1 \text{ m}}$$

or

$$\alpha = 256\ \mu \text{ rad.} \tag{13}$$

From the relation above and Figure 16, an expression for the magnitude of the range error Δx is derived.

$$\Delta x = (E_r)\ (\sin \alpha) \tag{14}$$

where

E_r = altitude from XXXE system

α = central angle whose maximum value after 60 seconds is 256 μrad (equation 13).

Upon series expansion of the sine function in equation 14 and retention of only the first two terms,

$$\Delta x = (E_r)\ (\alpha - \frac{\alpha^3}{3!})$$

or

$$\Delta x \approx 1.760 \text{ m.} \tag{15}$$

This is the maximum expected error in range, for it is the value calculated after maximum flight time and using maximum altitude value.

Now to obtain an expression for the relation and magnitude of the altitude error Δy (Fig. 10), we note from central angle α between displacements of earth's radius that

$$A = (r)\ (\cos \alpha) \tag{16}$$

where

A = adjacent leg of right triangle α

r = constant radius of earth.

Since α has the maximum value given by equation 13,

then

$$A = 6373383.908 \text{ m.} \tag{17}$$

Also from Figure 16,

$$A + \Delta y = r$$

or

$$\Delta y = r - A \tag{18}$$

and

$$\Delta y \approx 0.192 \text{ m.} \tag{19}$$

This is the maximum expected error in altitude, for it is the value calculated after maximum flight time and using the minimum value for A.

Having determined maximum magnitudes of the range and altitude approximation errors, we recall expressions 10 and 11 relating approximation errors and measured values.

$$c_x = x_m - \Delta x$$

$$H = y_m + \Delta y$$

where c_x is the parameter which acceptably approximates the true range s and H is the parameter which acceptably approximates the true altitude E_r.

Therefore, if the range approximation error is determined and subtracted from the measured value of range in the flat earth system, we have a parameter c_x that gives a close approximation to the XXXE range value s. Likewise, upon determination and proper consideration of the altitude approximation error, we have a parameter H that gives a close approximation to the XXXE altitude value E_r.

The degree of approximation between c_x and s will now be determined. From Figure 16 and using expression 13,

$$c_x = (r)\ (\alpha - \frac{\alpha^3}{3!}). \tag{20}$$

Also

$$s = r\alpha. \tag{21}$$

Therefore

$$s - c_x = r\alpha - \left[(r)(\alpha - \frac{\alpha^3}{3!})\right] \tag{22}$$

and

$$s - c_x = r\frac{\alpha^3}{3!} \approx 1.631 \times 10^{-5}\ m$$

so c_x approximates the true range s to better than 0.017 mm.

In a similar manner, the degree of approximation between H and E_r may be determined. From Figure 16,

$$H = E_r \cos \alpha. \tag{23}$$

Then

$$E_r - H = E_r - (E_r \cos \alpha).$$

Upon series expansion of cos α and retention of the first two terms,

$$E_r - H = E_r\ (1 - \frac{\alpha^2}{2!}) \tag{24}$$

and after 60 seconds of flight time

$$E_r - H = .229 \times 10^{-3} \text{ m}$$

so H approximates the true altitude E_r to better than 0.23 mm.

The approximation errors, measured values, approximation parameters, and their relations are shown in Table III.

Another approximation results from the constant distance of separation between the origin of the vehicle coordinate system and the origin of the instrument coordinate system. For the present analysis, this distance is equal to one kilometer.

From Figure 17, the angle γ and the perpendicular directed distance ℓ

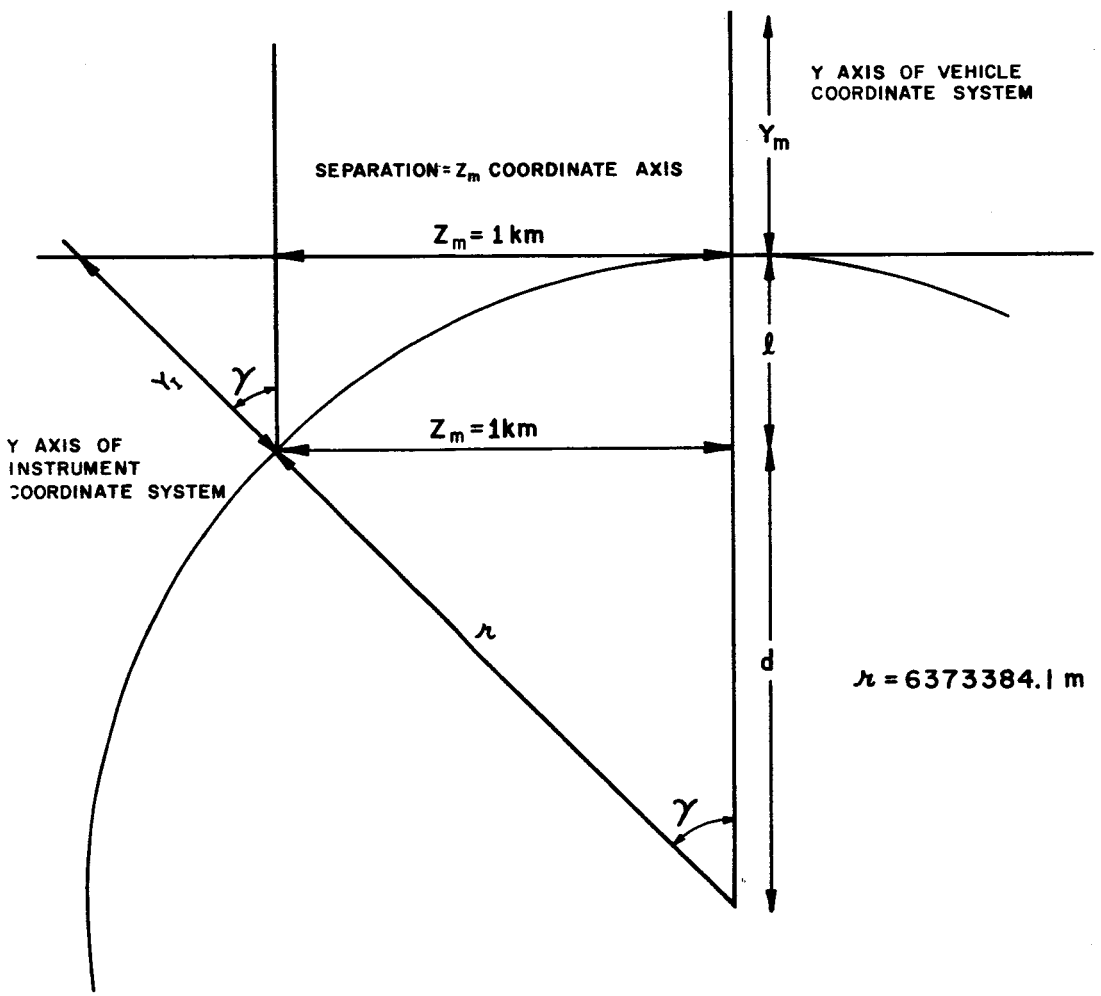

Figure 17. Constant Correction Because of Flat Earth Separation.

from the flat earth plane to the surface of the earth may be calculated as follows:

$$\sin \gamma = \frac{z_m}{r} \tag{22}$$

$$= \frac{1000 \text{ m}}{6373384.1 \text{ m}}$$

$$= 1.56 \times 10^{-4} \text{ rad.}$$

Also from Figure 17,

$$d = r \cos \gamma \tag{23}$$

$$= 6373384.0362 \text{ m}$$

where d is the adjacent leg of the triangle γ,

and

$$\ell = r - d \tag{24}$$

where ℓ is the directed distance from the flat earth plane to the earth's surface and

$$\ell \approx 63.8 \text{ mm.}$$

If system orthogonality is to be preserved, this constant error must be appropriately accounted for in the positioning of the instrument system.

E. FUTURE PLANS

Additional typical readouts from Saturn V, SA-9, and others will be studied in an effort to secure a better feeling for the range of variations to be expected in the instrument parameters.

Additional approximation analyses will be performed on all cases of typical values obtained from the readouts described.

Analytical expressions for the angular velocities and angular accelerations of θ and φ will be derived, and a computer program will be developed to test the accuracy of these expressions.

TABLE III. APPROXIMATION PARAMETERS

Measured values obtained from instrument system	Correction parameters calculated from system geometry	Approximation parameters whose values are acceptably close to those found in XXXE system	Equations relating measured values, correction parameters, and approximation parameters	Degree of approximation
x_m = Ground range	Δx = correction parameter to ground range x_m	c_x = Acceptable approximation of range in XXXE system	$c_x = x_m - \Delta x$	c_x approximates ground range in XXXE system to better than 0.017 mm
y_m = Altitude	Δy = Correction parameter to altitude y_m	H = Acceptable approximation of altitude in XXXE system	$H = y + \Delta y$	H approximates altitude in XXXE system to better than 0.23 mm

The general doppler effect will be treated. The doppler beat frequency variation with time will be plotted for optical frequencies. The beat frequency as a result of various modulation frequencies will also be plotted.

An effort will be made to derive analytical expressions for the variation of the approximation errors with time.

SECTION IV. PRELIMINARY RANGE ANALYSIS FOR THE PRECISION OPTICAL TRACKING SYSTEM

By

Charles L. Wyman

A. INTRODUCTION

Basic radar range equations are developed, and the characterization of the equations when using coherent optical wavelengths is discussed. Application of the equations to the optical tracking system is considered, along with a brief discussion of attenuation of light beams by the atmosphere.

Background radiation is estimated based on unattenuated sunlight reflecting diffusely off the vehicle skin with a reflectivity of one.

Nomenclature

A	aperture area
I	intensity
P	power
λ	wavelength
D	directivity
d	diameter
θ	half power beam angle
R	range
ϕ	angle of incidence of ray to a corner reflector
σ	effective reflecting area of a corner reflector array
α	coefficient of attenuation

B. RADAR EQUATIONS (Ref. 5)

The following developments neglect the effect of atmosphere, which is considered later.

The intensity of an isotropic source is

$$I = \frac{P_s}{4\pi} . \tag{1}$$

If a source has direction, such as a radar beam or a beam of light, then the beam has an axial intensity I_0. In the case of coherent sources (e.g., radar sources and lasers) of power P_t,

$$I_0 \approx \frac{P_t A_t}{\lambda^2} \tag{2}$$

where A_t is the area of a circular antenna aperture and λ is the wavelength of the energy. This calculation assumes a diffraction limited antenna system. It also accounts for the fact that all of the energy is not concentrated within the half power beam width (Ref. 6). The diffraction pattern of a circular aperture has about 83 percent of the energy in the central spot and about 50 percent within the half power points.

In practice, this situation is very closely approached. The directivity of a beam may now be defined as

$$D_t = \frac{I_0}{I} . \tag{3}$$

The energy distribution of the central lobe of the diffraction pattern is very nearly Gaussian. A good approximation for the half power beam width is

$$\theta_t \approx \frac{\lambda}{d_t} \tag{4}$$

θ_t is in radians and d_t is the diameter of the antenna aperture in the same units as the wavelength. Directivity may now be related to beam width. Substituting equations 1 and 2 into equation 3 with $P_s = P_t$,

$$D_t = \frac{4 \pi A_t}{\lambda^2} \quad . \tag{5}$$

Substituting equation 4 into equation 5,

$$D_t = \frac{\pi^2}{\theta_t^2} \quad . \tag{6}$$

Knowledge of beam directivity enables a determination of the power density P_{dt} on a target at range R.

$$P_{dt} = \frac{P_t D_t}{4 \pi R^2} = \frac{P_t \pi}{4 \theta_t^2 R^2} \quad . \tag{7}$$

The derivation of range equations for the optical tracking system takes a radical departure from equations for conventional radar at this point. In a conventional radar system, the power reflected to the receiver is an inverse function of range to the fourth power and a function of some effective reflecting area based on a diffuse target that scatters the received energy in all directions. The optical tracking system utilizes retrodirective optical corner reflectors on the booster to turn the beam back on itself. The corner reflectors will redirect the received radiation back to the tracker with some new directivity D_{cr}, which may be estimated from a knowledge of the individual corner reflectors.

$$D_{cr} \cong \frac{4 \pi A_{cr} f(\phi)}{6 \lambda^2} \quad . \tag{8}$$

The factor of six occurs in the denominator of the equation because of multiple reflections off the three surfaces of the corner reflector; the reflections cause the reflector to appear as an array of six apertures, each having one-sixth the area of the whole reflector. Since these apertures are not circular, the equation is an approximation. Note that the directivity is a function of the angle of incidence ϕ of the energy. The variation in angle of incidence causes the reflecting surfaces to appear as projections of themselves. The smaller the projected area, the greater the divergence of the beam.

An array of reflectors oriented at different angles will serve as an effective reflecting area with an effective diffraction limiting aperture over the total angle of incidence required to fulfill the system specifications. This is indicated in the following equation:

$$D_a \cong \frac{4 \pi A_{cr} f(\phi_e) N}{6 \lambda^2} \tag{9}$$

where D_a is the directivity for the array, ϕ_e is the effective angle of incidence to the contributing reflectors in the array, and N is the number of reflectors contributing to the return beam.

Typically, an angle of incidence ϕ of $\pm$ 20 degrees causes a 50 percent reduction in reflecting area for a single corner reflector. If in the worst situation at least one corner reflector is at an angle of 20 degrees from the normal, then $f(\phi_e) = .50$ and $N = 1$. For this situation, the directivity is

$$D_a \approx \frac{4 \pi A_{cr} (.5)}{6 \lambda^2} . \tag{10}$$

Calculations for a corner reflector 5-cm in diameter and a wavelength of 0.6 μ follow

$$D_a \approx \frac{4 \pi \left(\frac{25 \pi}{4}\right) (.5)}{6 (0.6 \times 10^{-4})^2} = 0.56 \times 10^{10}.$$

This figure corresponds to a beam divergence of 42 μ rad or 8.4 arc seconds. This results in a substantial gain in return signal compared with reflection off a diffuse target. The directivity may be expressed in terms of the beam divergence θ_a of the array

$$D_a = \frac{\pi}{\theta_a^2} . \tag{11}$$

We may now calculate the energy density at the receiver.

$$P_{dr} = \frac{P_{dt} A_{cr} f(\phi_e) N D_a}{4 \pi R^2} . \tag{12}$$

By substituting

$$\sigma = A_{cr}\, f\,(\phi_e)\; N \tag{13}$$

where σ is the effective reflecting area of the corner reflector array, and calculating on the basis of transmitted and reflected beam divergences, equation 14 is obtained

$$P_{dr} = \frac{P_t\, \pi^2\, \sigma}{16\, \theta_t^{\,2}\, \theta_a^{\,2}\, R^4}. \tag{14}$$

Thus, the use of the corner reflectors on the vehicle results in a system gain in received signal that is about 5 orders of magnitude greater than that which would be received off a diffuse target.

Also note that the return beam is so narrow that at close ranges it will not fill the receiver aperture. This occurs for ranges such that

$$R\theta_a < d_r \tag{15}$$

where d_r is the receiver diameter. Now, the power received for close range and long range may be calculated. The power received at close range is

$$P_r = P_{dt}\, \sigma. \tag{16}$$

For long range

$$P_r = P_{dr} A_r = \frac{P_t\, \pi^2\, \sigma\, A_r}{16\, \theta_t^{\,2}\, \theta_a^{\,2}\, R^4} \tag{17}$$

where A_r is the area of the receiver.

C. ATMOSPHERIC EFFECTS

A beam of electromagnetic energy being propagated through a medium is attenuated according to

$$I = I_i\, e^{-\alpha R} \tag{18}$$

where I_i is the initial intensity, α is the coefficient of attenuation, and R is the range. The two factors that contribute to the attenuation are absorption and scattering. At visible wavelengths, absorption is negligible relative to scattering and may be ignored for our purposes. Scattering varies markedly with atmospheric conditions, and an estimation of the magnitude and variation of α is important to range calculations. Scattering also varies to the inverse of the fourth power of the wavelength. The theory of scattering is developed in several references (Refs. 6, 7, and 8) and is not considered in this report.

Past researchers have measured attenuation as a function of wavelength over various path lengths and environmental conditions. Reference 9 shows the results of many of these measurements graphically. An estimate of the magnitude and variation of α from such graphs is probably the best means presently available. Later, experimental measurements using a laser will be made. Table IV shows percent transmission at 0.6 μ wavelength at various ranges and environmental conditions. These values are taken from graphs of Reference 9.

TABLE IV. ATMOSPHERIC TRANSMISSION

Range	Percent Transmission	Temperature	Relative Humidity	Precipitable Water Vapor	Daylight Visual Range
5.5 km	32%	28° C	73%	9.4 cm	19 km
5.5 km	41%	6° C	66%	2.2 cm	24.2 km
5.5 km	70%	22° C	51%	4.18 cm	60 km
16.25 km	21%	9° C	48%	5.2 cm	39 km
16.25 km	31%	16° C	41%	6.7 cm	54 km
16.25 km	50%	20° C	53%	15.1 cm	60 km
16.25 km	12%	26° C	82%	27.7 cm	22 km
16.25 km	2%	33° C	59%	37 cm	19 km

By using the transmittance values from the table and calculating attenuation per kilometer distance, note that α varies from 0.04 to 0.25. The range equations must be corrected for attenuation. The total transmittance path is 2 R; therefore, the range equation becomes

$$P_r = \frac{P_t \pi^2 \sigma A_r e^{-\alpha 2R}}{16 \theta_t^2 \theta_a^2 R^4}. \qquad (19)$$

Calculating the ratio of maximum transmission at short range to minimum transmission at long range indicates the variation in signal that must be tolerated. This calculation was made using a minimum range of 3 km, a maximum range of 10 km, $\theta_t = 150\ \mu$ rad, $\theta_a = 40\ \mu$ rad, $\sigma = 2 \times 10^{-3}$, and $A_r = 2 \times 10^{-2}$. The calculation indicated a dynamic variation of 10^4. A variation in signal of this magnitude will probably necessitate automatic gain control in the receiver. Note that this calculation is for long term variation in which environment plays a part. The problem is somewhat alleviated for short term variation (several minutes). A calculation using a constant α indicates a worst case dynamic variation of signal of about 3×10^3 and a best case variation of about 200.

D. BACKGROUND RADIATION

The worst background to be encountered in the tracking system will be direct sunlight reflecting off the skin of the vehicle. Since the receiver field of view is small, this background will normally fill it. Normally the vehicle is painted white and will appear as a diffuse surface. The worst case situation arises when the vehicle is several kilometers high and the sunlight strikes it with little atmospheric attenuation.

Narrow band optical filters will be used to discriminate against background; therefore, background calculations may be based on the solar radiation flux in the spectral region of interest. For this first approach to the problem, values of solar radiation of 6000 Å over a 10 Å band will be assumed. Reference 10 gives a radiation value of 183×10^{-7} J cm^{-2} Å^{-1} s^{-1}. This corresponds to 183 μ watts/cm^2 over the spectral region of interest. The background radiation incident on the receiver is

$$P_b = \frac{A_b P_{db} \times 2 \times A_r}{4 \pi R^2} \qquad (20)$$

where A_b is the area of the background in the field of view and P_{db} is the background density previously calculated. Note that A_b is a function of the receiver field of view and the range squared. Also, for optimum operation, the receiver field of view is equal to transmitter beam angle θ_t. The equation becomes

$$P_b = \frac{P_{db} A_r \theta_t^2}{32}. \tag{21}$$

With 15 cm receiver optics, $P_{db} = 183 \times 10^{-6}$ watts/cm^2, and $\theta_t = 150\ \mu$ rad, we find that the $P_b \approx 10^{-10}$ watts. Using a 50-milliwatt transmitter and the same figures previously calculated, a minimum signal of $P_r = 230 \times 10^{-10}$ watts is obtained. Thus, the normal background that will be encountered during tracking is not a problem. However, during acquisition, the vehicle plume or even the sun or moon may come into the field of view. This problem will be considered in a later report.

E. CONCLUSIONS

The percentage of energy that is returned to the receiver is very high compared to conventional radar. The high directivity of the transmitter contributes heavily to the increased signal. Furthermore, the use of corner reflectors on the vehicle adds many orders of magnitude to the signal. Altogether, improvement in signal-received to signal-transmitted ratio amounts to more than 10^8 over conventional systems.

There are several advantages to working with optical carrier frequencies. First, the tremendously increased signal is achieved with much smaller apertures. Second, the use of high frequencies and the increased directivity both work toward much greater precision of measurements. Third, this system is free of ground clutter and interference when operating near the horizon. Ground clutter alone makes it virtually impossible to use conventional radar for early launch phase tracking.

SECTION V. REFRACTIVE AND TURBULENCE EFFECTS OF THE EARTH'S ATMOSPHERE

By

Larry Hayes

A. INTRODUCTION

Light rays passing through the atmosphere are bent because of variations in the atmosphere's refractive index. To obtain true optical measurements of the position of a target, the amount of bending caused by the atmosphere must be determined.

Nomenclature

a	radius of earth
φ	true angular position
d	linear displacement along earth's surface
n	refractive index
n_o	refractive index at sea level
α	angle between earth's radius drawn to tracker and radius extended to target
ρ	atmospheric density
R	slant range
r	distance from center of earth to a point on the ray path
τ	angle formed between targets drawn to ray path at the tracker and the target
θ	angle between the tangent to the ray path and a line drawn normal to the earth's radius at the point where it intersects the ray

θ_o apparent elevation angle = value of θ at observation point

y_ρ 9296 meters

y height above earth's surface

B. DISCUSSION OF PROBLEM

In the simple case of refraction at the boundary of two layers of different refractive indices, light rays are bent toward the normal as the light passes from the medium of low refractive index to the medium of high refractive index (Fig. 18). The amount of bending depends on the change in refractive index. With a stack of layers (Fig. 19) where $n_o > n_1 > \ldots > n_n$, a light ray will be bent in succession at each interface. The total bending will be the sum of all the small changes in the direction of the ray. The path of the ray will look like the irregular curve in Figure 2.

Now for the problem of atmospheric bending, consider the atmosphere to be composed of a stack of layers with varying refractive indices. If each layer is assumed to have an infinitesimal thickness, $\Delta y \to 0$, the ray path will approximate a smooth curve (Fig. 20). In this figure a light ray is continuously bent as it travels through the atmosphere. The apparent direction of the ray at point zero is θ_o where θ_o is the angle between the horizontal and the tangent to the ray at point zero. The actual elevation angle is φ so that the angular elevation error is

$$\Delta\varphi = \theta_o - \varphi. \tag{1}$$

In any non-homogeneous medium, light rays will be bent in the direction of the gradient of the refractive index n. The amount of bending depends on the magnitude of the gradient. The density ρ of the atmosphere follows an approximately exponential decrease with height above the earth's surface. From Gladstone and Dale's law

$$n - 1 = (\text{constant})\,\rho\,. \tag{2}$$

The term (n - 1) also follows an exponential decrease with height and approaches a value of zero. This exponential model of the atmosphere accurately represents average atmospheric conditions. This model is used frequently in studies of atmospheric effects on electromagnetic radiation.

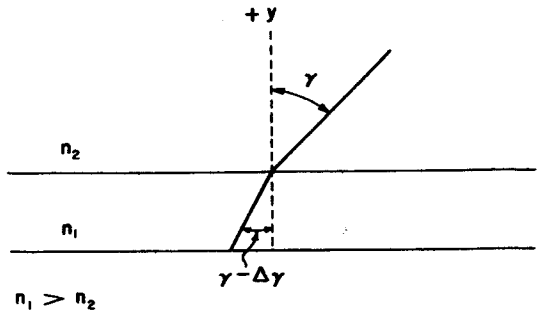

Figure 18. Refraction at a Boundary.

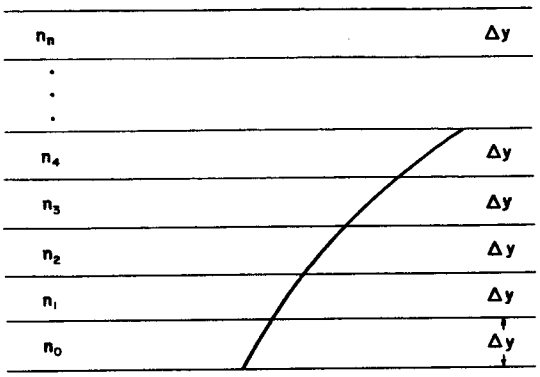

Figure 19. Refraction in a Stratified Medium.

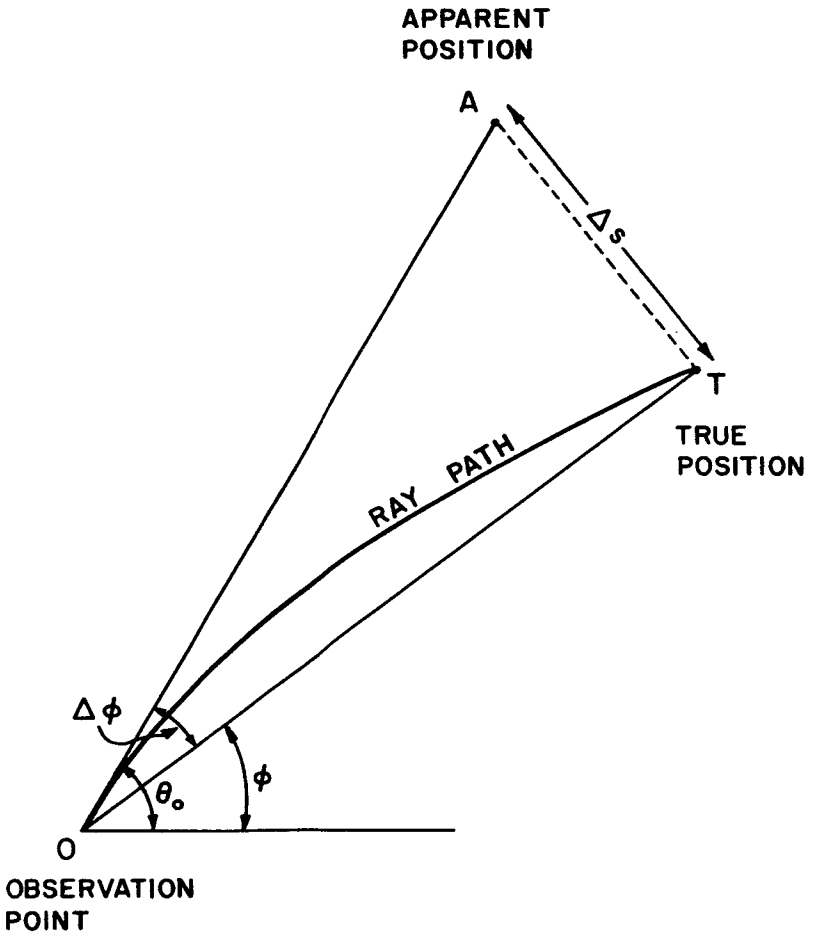

Figure 20. Atmospheric Refraction.

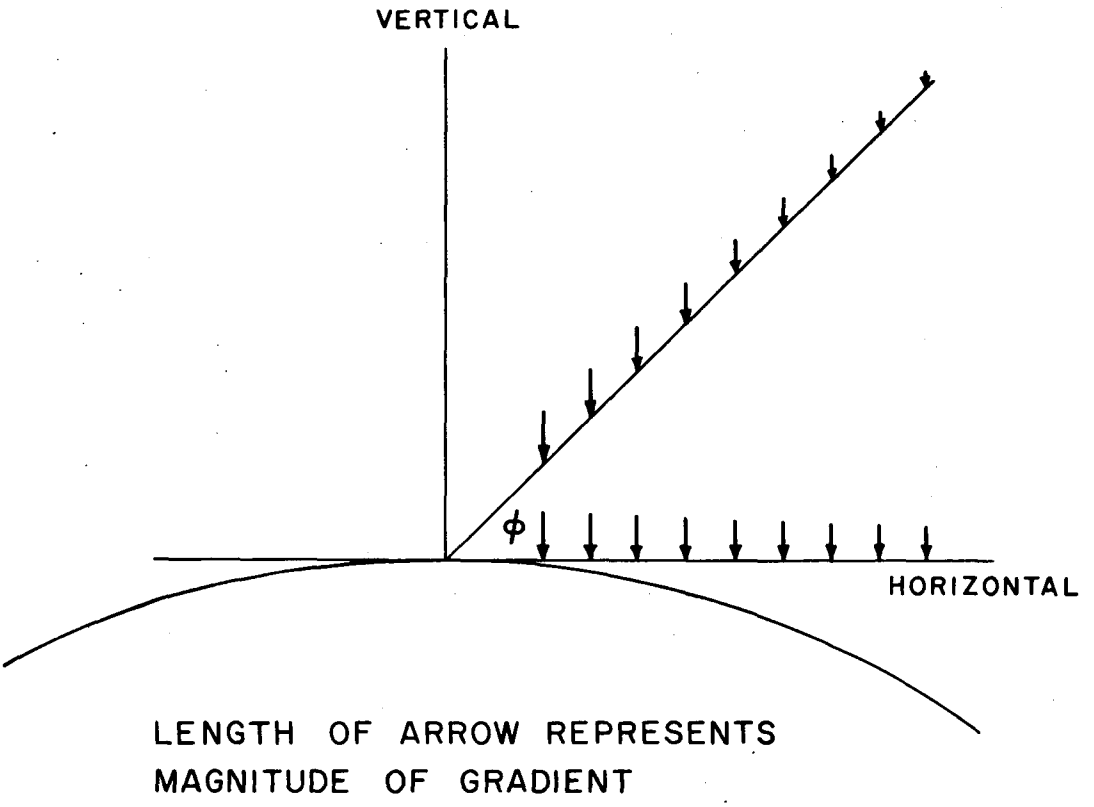

Figure 21. Probable Variation of the Refractive Index Gradient.

The refractive index changes rapidly near the earth's surface. Thus, the magnitude of the gradient of n is greater at low altitudes than at high altitudes. As a result, the gradient changes very slowly along a nearly horizontal path and rapidly along a path making some angle with the horizontal (Fig. 21). The amount of bending depends on the distance traveled, since the effect is cumulative. But for a given distance (slant range), the total bending for a nearly horizontal ray will be much greater than for a ray making a large angle with the horizontal.

The errors caused by atmospheric refraction can be divided into two categories. One is the steady-state component of the error and the second is the time varying component. The time varying component is caused by atmospheric turbulence and causes the error to fluctuate about a mean value, i.e., the steady-state component. Such factors as wind and heat waves contribute to the atmospheric turbulence. At present, only the steady-state component is considered. A first approximation is obtained by using average atmospheric conditions to calculate refraction errors. Later corrections can be made for local conditions.

C. CALCULATION FOR TYPICAL CASE

Several studies of atmospheric refraction have been reviewed. The equations for the amount of bending are given in Table V. All these studies used an exponential model for the decrease in refractive index. The following equation is used to calculate the total angular bending of the ray.

$$d\tau = - \frac{d_n}{n} \cot \theta, \qquad (3)$$

where τ = angular bending or angle between tangents to ray path at the two points in question.

θ = angle at any point on the ray between the tangent at that point and the normal to the earth's radius extended to that point (Fig. 22).

Equations for the angular elevation error, $\Delta\varphi$, were also derived in several reports (Refs. 11, 12,and 13).

The report by Perkin-Elmer (Ref. 13) is a comprehensive treatment of the problem of atmospheric refraction of optical frequency radiation. Their equation for calculating $\Delta\varphi$ is readily evaluated since it is not necessary to find a value for τ, the total angular bending. Also values for the variables, true elevation angle φ, and slant range R are easily obtained from available data. For these reasons, equation F from Table V,

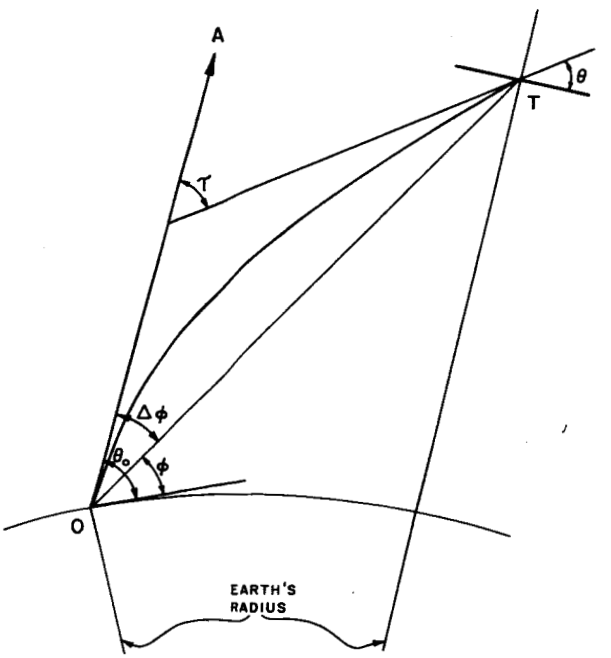

Figure 22. Problem Geometry.

TABLE V. BENDING EQUATIONS

	Total angular bending, τ	Error in observed elevation angle, $\Delta\varphi$
Bean and Cahoon	A) $d\tau = -\frac{dn}{n}\cot\theta$	C) $\Delta\varphi = \tau - \arctan \dfrac{\frac{n}{n} - \cos\tau - \sin\tau\tan\theta_0}{\sin\tau - \cos\tau\tan\theta_0 + \frac{n_1}{n}\tan\theta}$
Bean and Thayer	B) $d\tau = -\frac{dn}{n}\cot\theta$	
W. M. Smart	D) $d\tau = -\frac{dn}{n}\cot\theta$	where "0" and "1" subscripts represent values of the observation point and the target, respectively
Fannin and Jehn		E) $\Delta\varphi = \cot\varphi \quad (n_o - n_o') - \frac{1}{Z_1}\int_o^{Z_1}(n-n')\,dz$
Perkin-Elmer		where $z = 1 - \sin\theta_0 \quad \sin^2\theta_0 + (r/r_0)^2 - 1 \Big)^{-\frac{1}{2}}$
		Primes represent reference atmosphere conditions
		F) $\Delta\varphi = \dfrac{(n_0 - 1)\, y_\rho \cot\varphi}{R \sin\varphi}\left(1 - e^{\frac{-R\sin\varphi}{y_\rho}}\right) - n_0 - 1)\cot\varphi$
		where: y_ρ = 9296 meters
		R = slant range

$$\Delta\varphi = \frac{(n_o - 1)\, X_\rho \cot\varphi}{R \sin\varphi} \left[1 - e^{-\frac{R \sin\varphi}{y_\rho}}\right] - (n_o - 1) \cot\varphi \qquad (4)$$

where n_o = refractive index to sea level, was used to calculate values of $\Delta\varphi$ (Fig. 22). Values of ϕ and R were taken from the same typical Saturn V trajectory used in Section III.

An exponential model of the atmosphere was used such that

$$\frac{\rho}{\rho_o} = e^{-y/y_\rho},$$

ρ = density of air,

ρ_o = value of ρ at sea level

y = height above earth's surface.

y_ρ is defined as the point where $\rho = \frac{1}{e}\rho_o$. The value of y_ρ obtained from standard atmosphere tables is 9296 meters.

After the elevation angular error has been determined, a correction for position can also be obtained. Figure 20 shows that the error in position, Δs, is given by

$$\Delta s \cong R\Delta\phi. \qquad (5)$$

Values of Δs were calculated from equation 5. Graphs of $\Delta\varphi$ and Δ_s versus time are given in Figures 23 and 24. Figure 23 shows that the elevation error, $\Delta\varphi$ decreases slightly for the first 40 seconds of flight. The elevation error increases with increasing slant range R for a given elevation angle. But as the elevation angle increases, the ray passes through a decreasing refractive index gradient. Therefore, for a given slant range, the elevation error decreases with increasing elevation angle. As both the range angle and elevation angle are increasing functions of time, the effects of one tends to offset the effects of the other. At about 40 seconds, the value of the elevation angle approaches a constant value. The rapid increase in slant range accounts for the sharp rise in elevation error $\Delta\varphi$ after 40 seconds. The error in height Δs is almost constant over the first 20 seconds of flight because of a slightly decreasing $\Delta\varphi$ and a slowly increasing R. The sharp increase in R after 20 seconds causes the jump in the values of Δs.

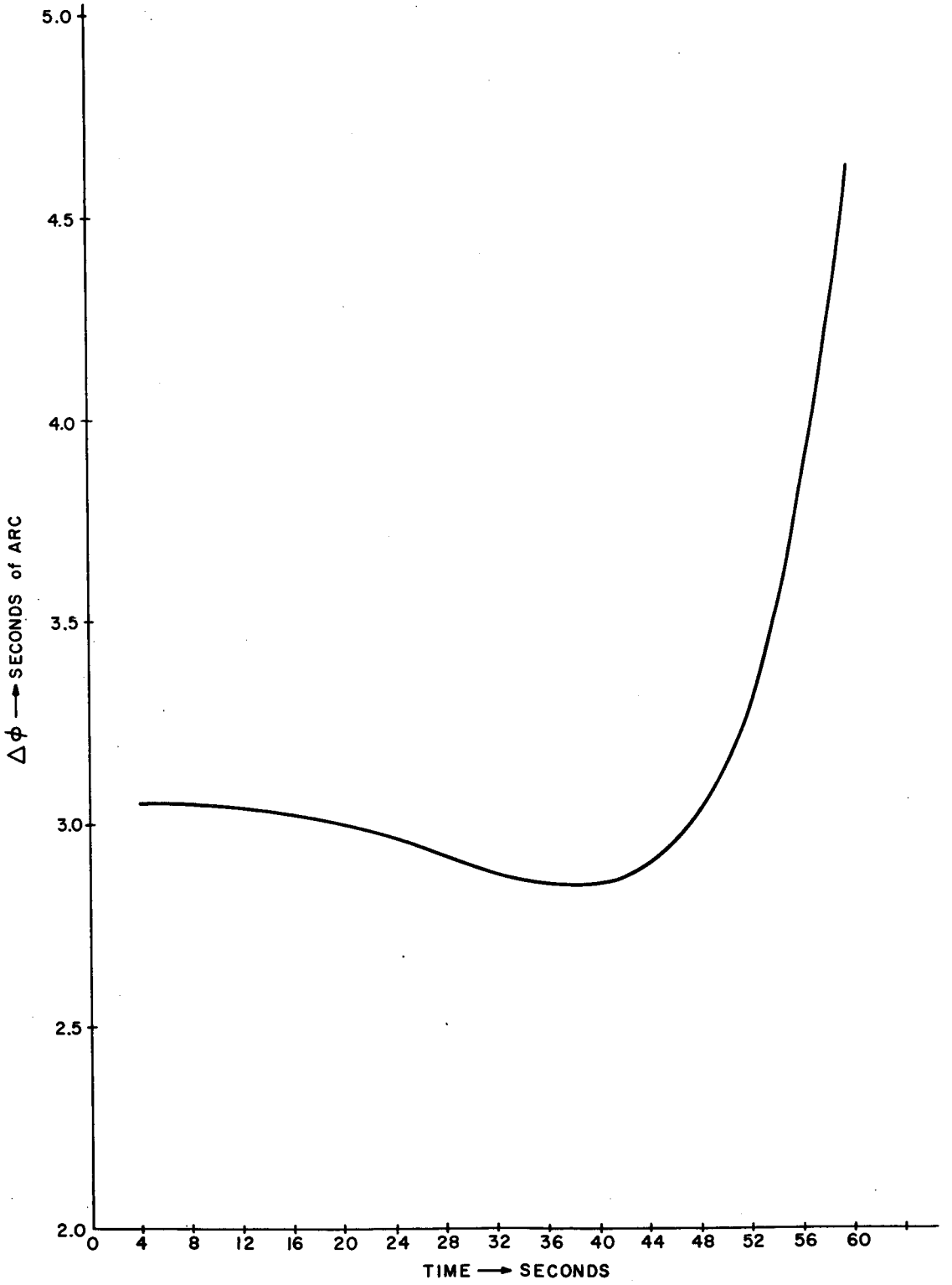

Figure 23. $\Delta \phi$ Versus Time.

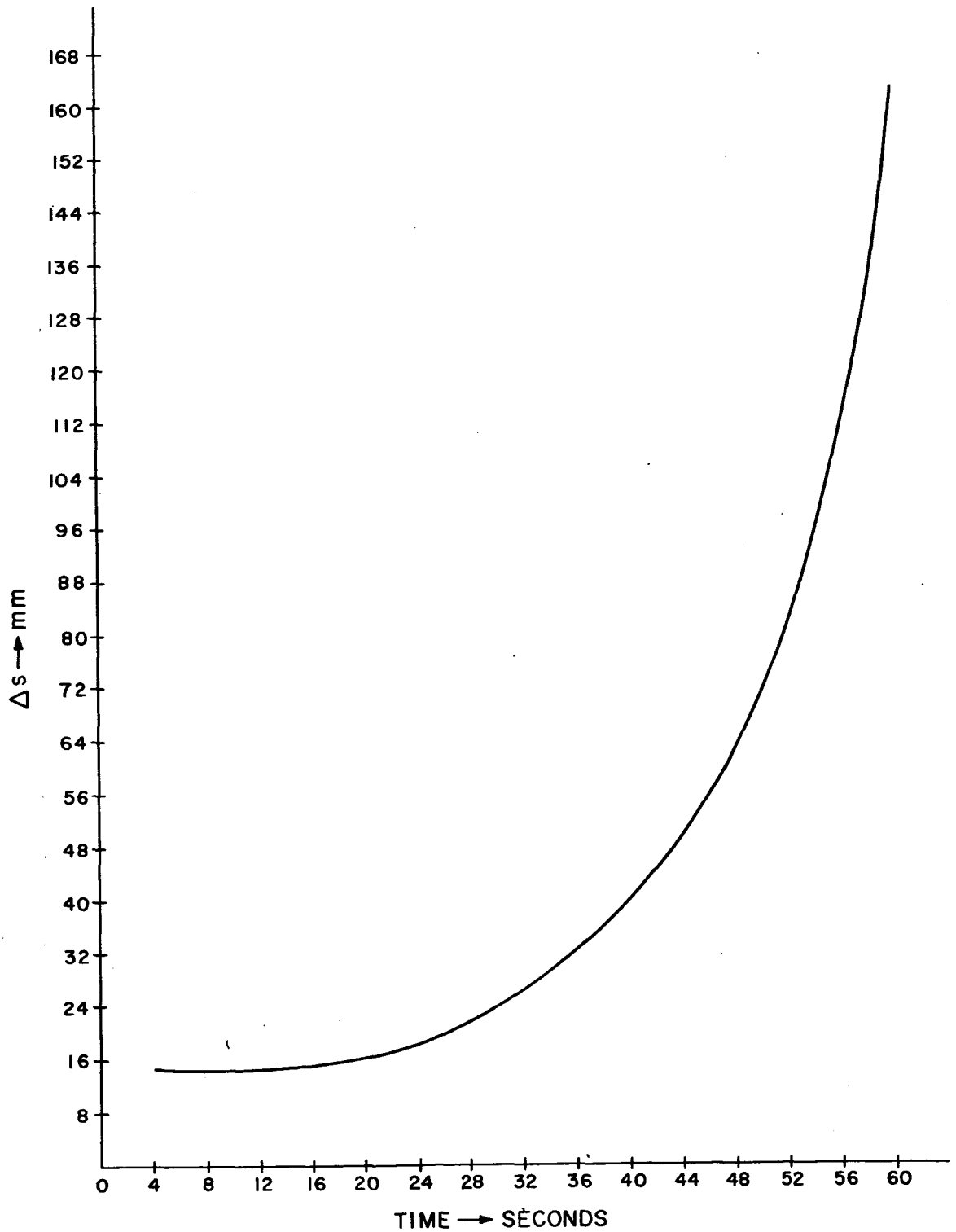

Figure 24. △s Versus Time.

D. CONCLUSIONS

It is generally agreed that the exponential model of decreasing the refractive index closely approximates average atmospheric conditions. Higher accuracy can be obtained by experimental determination of local conditions. Note that the values of $\Delta\varphi$ and Δs given in Figures 23 and 24 are for a single typical Saturn V vehicle trajectory. These graphs can be used to obtain a feeling for the errors involved. To determine the error for any given point in the atmosphere, the error must be given as a function of elevation angle and slant range.

E. FUTURE PLANS

The effect of atmospheric turbulence is a major problem which must be considered in an optical tracking system. Since turbulence generally causes random fluctuations, statistical methods must be used to investigate this problem. A study will be made to determine the exact nature and magnitude of the errors introduced by turbulence. Also, an effort will be made to determine an accurate analytical expression for the error caused by the atmosphere. After computing this error, tables and graphs will be prepared to correct observed angles.

SECTION VI. TRACKING MOUNT SERVO SYSTEM

By

John M. Gould

A. INTRODUCTION

The problem considered in this section is the definition of the preliminary design parameters for the vehicle tracking platform servo. The design is based on the listed specifications. Since the noise statistics of the error detector are not available, the servo bandwidth has been minimized, while at the same time the other conflicting requirements such as response time and high static accuracy have been satisfied.

The control actuator will be an electric torquer to avoid the attendant backlash and friction of a motor and gear drive combination. Angle encoders, whose outputs may be processed to provide rate feedback similar to that of a dc tachometer, will be used about the elevation and azimuth axes.

The control system will be a type one servo with tachometer feedback. It will yield the desired static accuracy in the presence of high breakaway friction and will operate at a very small dynamic error with good stability.

Nomenclature

s	Laplace operator	rad/s
t	time	s
t_b	time at breakaway	s
u	unit step operator	
$F(s)$	position error signal compensation of tachometer stabilized loop	
I	torquer current	A
$\|I\|$	magnitude of the torquer current	A
J	inertia at torquer shaft	kg m^2

K_e	back emf of torquer	V/rad/s
K_t	torquer sensitivity	m N/A
K_t/R	torquer sensitivity	m N/V
K_θ	position error signal gain of tachometer stabilized loop	V/V
$K^*_{\dot{\theta}}$	gain of closed rate loop	V/V
K°_θ	rate loop error signal gain	V/V
L	self inductance of torquer	H
$\frac{L}{R}$	torquer time constant	s
R	dc resistance of torquer	ohms
T_s	static friction torque (total)	m N
V	torquer applied voltage	V
V_b	torquer applied voltage for breakaway	V
B_t	tachometer sensitivity	V/rad/s
e_θ	position loop error	rad
e_{θ_s}	static position error (static accuracy)	rad
e°_θ	rate loop error signal	V
Z	damping ratio	
w_f	torquer control winding break frequency	rad/s
w_m	dominant torquer break frequency	rad/s

$\overset{*}{\theta}$	commanded servo angular position	rad
θ	angular position of torquer shaft	rad
$\overset{*}{\theta}_0$	servo rate command	rad/s
$\overset{*}{\dot{\theta}}$	rate loop command signal	V
$\dot{\theta}$	angular velocity of torquer shaft	rad/s
$\overset{*}{\ddot{\theta}}$	servo acceleration command	rad/s^2
$\ddot{\theta}$	angular acceleration of torquer shaft	rad/s^2

B. SPECIFICATIONS

1. Platform load - 136 kg
2. Maximum elevation angle - +90 deg
3. Minimum elevation angle - -10 deg
4. Maximum commanded acceleration - 1 deg/s^2
5. Maximum position error - 20 arc sec
6. Maximum commanded velocity - 5 deg/s
7. Moment of inertia about elevation axis - 16.3 kg m^2
8. Moment of inertia about azimuth axis - 163 kg m^2

C. TYPICAL COMPONENT CHARACTERISTICS

1. Torquer

   a. Back emf - 12 V/rad/s

   b. Sensitivity (K_t/R) - .136 mN/V

   c. Torquer time constant ($\frac{L}{R}$) -0.04 s

2. Tachometer

Sensitivity - 120 V/rad/s

3. Motor Drive Amplifiers

a. Elevation amplifier gain - 2.25 V/V ($K^{\bullet}_{\theta_x}$)

b. Azimuth amplifier gain - 22.5 V/V ($K^{\bullet}_{\theta_z}$)

D. DETAILED SYNTHESIS

The control problems of both the elevation and the azimuth axes will be studied in parallel. Parameters that are not common to both axes will be denoted by the subscripts x and z for elevation and azimuth, respectively.

1. Torquer Equations

Figure 25 is a general block diagram of the servo loop.

$$K_e \frac{d\theta}{dt} + Ri + L \frac{di}{dt} - v\ (t) = 0 \qquad (1)$$

$$J \frac{d^2\theta}{dt^2} - K_t\ iu\ (\Delta) = 0 \qquad (2)$$

where $u\ (\Delta T) = 0$ for $\Delta T < 0$ (3)

$u\ (\Delta T) = 1$ at $\Delta T \geq 0$

$$\Delta T = \left| K_t\ i \right| - T_s \qquad (4)$$

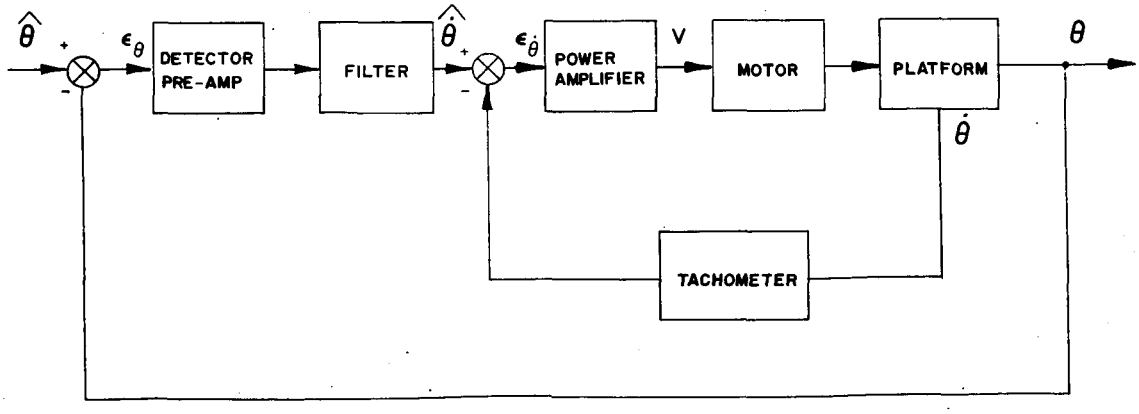

Figure 25. Overall Servo Loop.

Solving equation 4 for the current at breakaway $(t - t_b)$ necessary to overcome the static friction torque (T_s),

$$\Delta T = 0 \tag{5a}$$

$$\left| i\,(t_b) \right| = \frac{T_s}{K_t} \quad . \tag{5b}$$

At $\frac{d\theta}{dt} = 0$, the Laplace transform of the current transient in equation 1 becomes for no initial current

$$I\,(s) = \frac{1}{L} \quad \frac{V_b\,(s)}{(S + R/L)} \quad . \tag{6}$$

The current response to a step increment $V_b\,u\,(t)$ in the voltage is therefore

$$I\,(s) = \frac{V_b}{L} \quad \frac{1}{s(s + R/L)} \tag{7}$$

$$\text{and} \quad i\,(t) = \frac{V_b}{R} \quad (1 - e^{\frac{-Rt}{L}}) \tag{8a}$$

$$\text{for} \quad 0 < t < t_b \,. \tag{8b}$$

Therefore at time $t = t_b$

$$\left| i\,(t_b) \right| = \frac{T_s}{K_t} = \left| \frac{V_b}{R} \quad (1 - \epsilon^{\frac{R}{L}\,t_b}) \right| \,. \tag{9}$$

Solving equation 9 for the voltage increment necessary for breakout at $t = t_b$,

$$V_b = \frac{T_s \quad R}{K_t\,(1 - \epsilon^{\frac{-R}{L}\,t_b})} \,. \tag{10}$$

Rearranging equation 10, the time increment required for breakout is

$$t_b = \frac{L}{R} \quad \ln \quad \frac{K_t \quad V_b}{K_t V_b - RT_s} \,. \tag{11}$$

In the case of continuous signal operation, equations 5b and 10 define, respectively, the current and voltage necessary for breakaway. Equation 11 specifies the time increment necessary to overcome the friction torque.

Figure 26 represents the torquer equations in block diagram form.

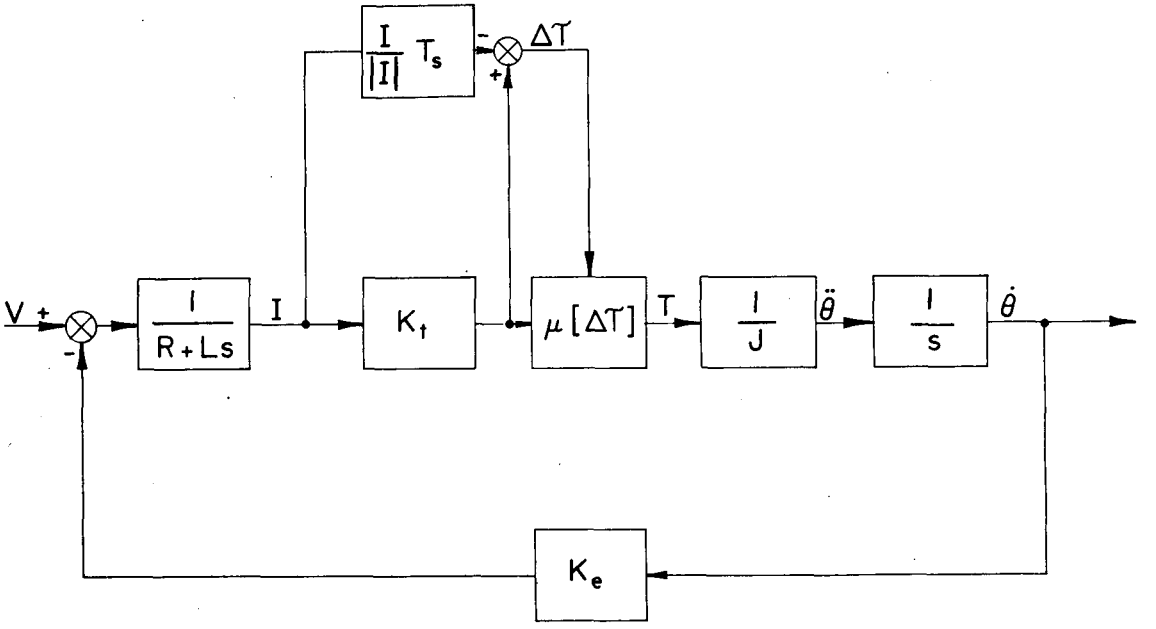

Figure 26. Torquer Block Diagram.

2. Tachometer Stabilized Loop

Subsequent to breakaway ($\Delta T > 0$), the transformed torquer equations 1 through 4 may be compactly stated as follows.

$$\begin{vmatrix} K_e & R + LS \\ JS & -K_t \end{vmatrix} \cdot \begin{vmatrix} \dot{A}(s) \\ I(s) \end{vmatrix} = \begin{vmatrix} V(s) \\ 0 \end{vmatrix} . \qquad (12)$$

Using equation 12, the transfer function of the torquer is

$$\frac{\dot{\theta}(s)}{V(s)} = \frac{K_t / LJ}{s^2 + \frac{sR}{L} + \frac{K_e K_t}{LJ}} . \qquad (13a)$$

This may be stated in the general form,

$$\frac{\dot{\theta}(s)}{V(s)} = \frac{w_h^2 / K_e}{s^2 + 2Z_h w_h s + w_h^2} . \qquad (13b)$$

where $$w_h^2 = \frac{K_e K_t}{JL} = \frac{K_e K_t R}{JRL} = \frac{12}{16.3} \times 0.136 \times 25 = 2.5\ (\text{rad/s})^2 \quad (13c)$$

$$w_{h_x}^2 = 2.5\ (\text{rad/s})^2 \quad (13d)$$

$$w_{h_z}^2 = \frac{12}{163} \times 0.136 \times 25 = 0.25\ (\text{rad/s})^2 \quad (13e)$$

$$w_{h_x} = 1.58\ (\text{rad/s}) \quad (13f)$$

$$w_{h_z} = 0.5\ \text{rad/s} \quad (13g)$$

and

$$Z_h = \frac{R/L}{Zw_h} \quad (14a)$$

$$Zh_x = \frac{25}{2 \times 1.58} = 7.9 \quad (14b)$$

$$Z_{h_z} = \frac{25}{2 \times 0.5} = 25. \quad (14c)$$

The roots of equation 13b are

$$S_1 = w_h\,(-Z_h + \sqrt{Z_h^2 - 1}) \quad (15a)$$

and

$$S_2 = w_h\,(-Z_h - \sqrt{Z_h^2 - 1}). \quad (15b)$$

For large damping ratios, Z_h, equations 15a and 15b may be approximated as follows.

$$S_1 \cong -2Z_h w_h = \frac{-R}{L} = -w_f \quad (16a)$$

$$S_2 \cong \frac{-w_h}{2Z_h} = \frac{-w_h^2}{w_f} = \frac{-K_e K_t}{JR} = -w_m \quad (16b)$$

$$w_{f_x} = 2 \times 7.9 \times 1.58 = 25\ \text{rad/s} \quad (16c)$$

$$w_{m_x} = \frac{1.58}{2 \times 7.9} = 0.1 \text{ rad/s} \tag{16d}$$

$$w_{f_z} = 2 \times 25 \times 0.5 = 25 \text{ rad/s} \tag{16e}$$

$$w_{m_z} = \frac{0.5}{2 \times 25} = 0.01 \text{ rad/s}. \tag{16f}$$

Also for large damping ratios, the transfer function of the torquer (equation 13a) may be written as

$$\frac{\dot{\theta}(s)}{V(s)} = \frac{1}{K_e} \frac{w_m}{S+w_m} X \frac{w_f}{S+w_f} . \tag{17}$$

Since w_f is so much larger than w_m, equation 17 may be reduced even further for all practical purposes.

$$\frac{\dot{\theta}(s)}{V(s)} = \frac{1}{K_e} \frac{w_m}{S+w_m} . \tag{18}$$

Using the torquer transfer function given by equation 18, the detailed block diagram of the tachometer stabilized loop is shown in Figure 27.

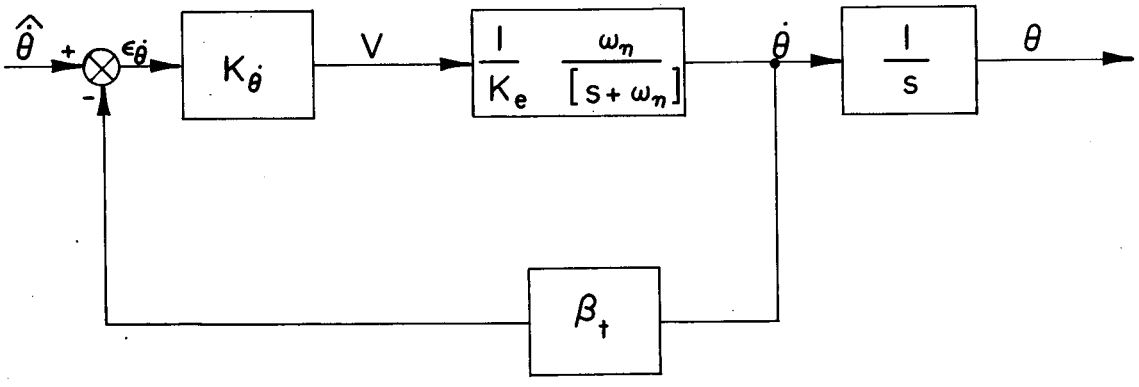

Figure 27. Tachometer Stabilized Loop.

$$\frac{\dot{\theta}(s)}{\dot{\theta}^*} = \frac{K \dot{\theta} w_m}{K_e (S+w_m) + K_{\dot{\theta}} w_m B_t} \tag{19a}$$

$$\frac{\dot{\theta}\,(s)}{\overset{*}{\dot{\theta}}\,(s)} = \frac{w_m K_{\dot{\theta}}/K_e}{S+w_m+B_t w_m K_{\dot{\theta}}/K_e} . \tag{19b}$$

Let $$w_{\dot{\theta}} = w_m (1 + B_t K_{\dot{\theta}}/K_e) \tag{20}$$

and $$\overset{*}{K}_{\dot{\theta}} = w_m K_{\dot{\theta}}/w_{\dot{\theta}} K_e . \tag{21}$$

Substituting equations 20 and 21 in equation 19, the loop transfer function reduces to

$$\frac{\dot{\theta}\,(s)}{\overset{*}{\dot{\theta}}\,(s)} = \overset{*}{K}_{\dot{\theta}}\, w_{\dot{\theta}}/\,(s + w_{\dot{\theta}}) \tag{22a}$$

where

$$w_{\dot{\theta}_x} = 0.1\ (1 + 120 \times 2.25/12) = 2.35 \text{ rad/s} \tag{22b}$$

$$w_{\dot{\theta}_z} = 0.01\ (1 + 120 \times 22.5/12) = 2.22 \text{ rad/s} \tag{22c}$$

$$\overset{*}{K}_{\dot{\theta}_x} = 0.1 \times 2.25/2.35 \times 12 = 0.00797 \tag{22d}$$

$$\overset{*}{K}_{\dot{\theta}_z} = 0.01 \times 22.5/2.22 \times 12 = 0.00844 . \tag{22e}$$

Figure 28 shows the complete servo loop.

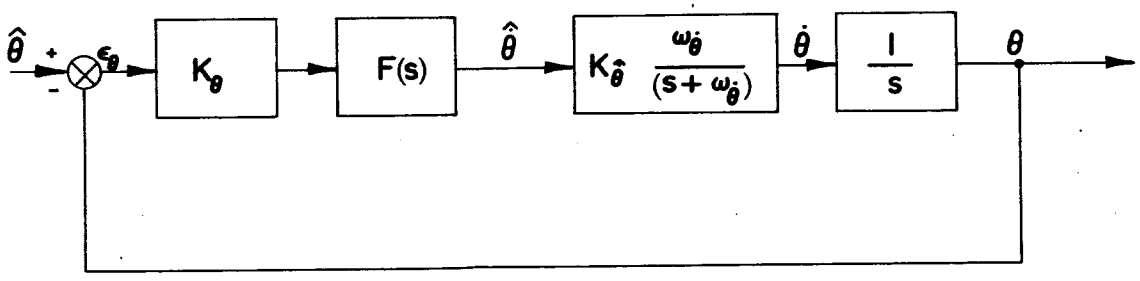

Figure 28. Complete Servo Loop.

3. Command Limitations

Consider the command sinusoidal motion,

$$\overset{*}{\theta} = (A) \sin wt. \tag{23}$$

The command velocity for this motion is

$$\overset{*}{\dot{\theta}} = \frac{d\overset{*}{\theta}}{dt} = (w\,A) \cos wt. \tag{24a}$$

The command acceleration for this motion is

$$\overset{*}{\ddot{\theta}} = \frac{d\overset{*}{\dot{\theta}}}{dt} = -(w^2 A) \sin wt. \tag{24b}$$

The specification defines the maximum values of velocity (w A) and acceleration (w^2 A) as being 5 deg/s and 1 deg/s^2, respectively. Thus, the maximum amplitudes of required motion will be limited by

$$w\,A \leq 5 \text{ deg/s} \tag{25a}$$

or

$$A \leq \frac{5}{w} \text{ deg} \tag{25b}$$

and

$$w^2 A \leq 1 \text{ deg/s}^2 \tag{25c}$$

or

$$A \leq \frac{1}{w^2} \text{ deg.} \tag{25d}$$

These two limitations on amplitude (A) cross over at w = 0.2 rad/s. The tracking error throughout these maximum motions must not exceed 20 arc seconds as per the specifications.

Figure 29 depicts the limitations of A with frequency and the allowed error level. From Figure 29,

$$\frac{\overset{*}{\theta}}{e} = \frac{1000}{w} \times \frac{0.2}{w + 0.2} . \tag{26}$$

Consider the general servo equation where

$$\theta = \frac{KG\ \overset{*}{\theta}}{1 + KG} \tag{27}$$

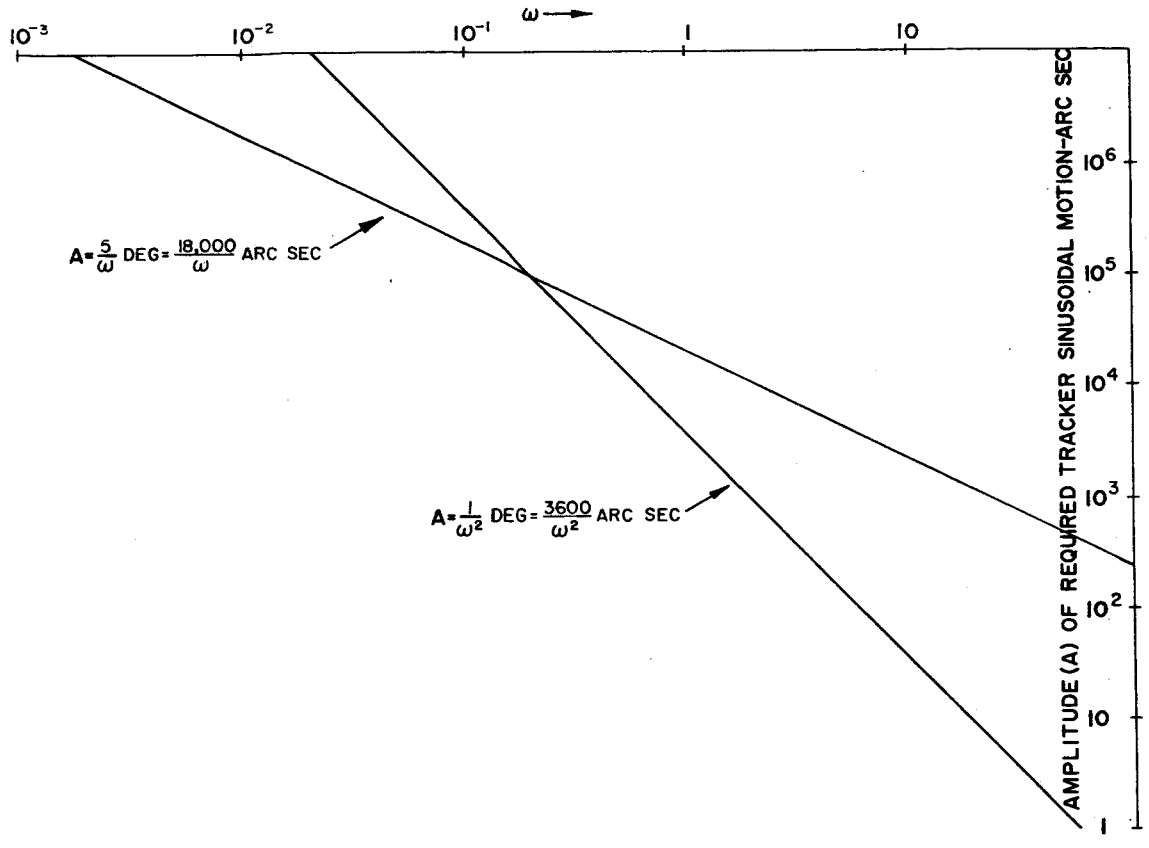

Figure 29. Limits of Required Tracker Motion.

and

$$\frac{\overset{*}{\theta}}{e} = 1 + KG. \tag{28}$$

The system specifications will be satisfied by

$$1 + KG \overset{\geq}{=} \frac{1000}{s} \times \frac{0.2}{s + 0.2} . \tag{29}$$

A good equation that satisfied equation 29 was found to be

$$1 + KG = \frac{(s^2 + 28.3s + 400)\ (s + 28.1)}{s\ (s + 0.2)\ (s + 56.2)} . \tag{30}$$

Solving equation 30 for KG yields

$$KG = \frac{1180\ (s + 9.5)}{s(s + 0.2)\ (s + 56.2)} . \tag{31}$$

4. Compensating Filter

Referring to Figure 28 and equation 22, it can be seen that the open loop transfer function is

$$\frac{\theta}{\epsilon_\theta} = K_\theta F(s) K_{\dot{\theta}}^{*} \frac{w_{\dot{\theta}}}{s(s+w_\theta)} \tag{32a}$$

$$\frac{\theta_x}{e_\theta} = K_{\theta_x} F(s)_z \frac{0.00797 \times 2.35}{s(s+2.35)} \tag{32b}$$

$$\frac{\theta_z}{\epsilon_\theta} = K_{\theta_z} F(s)_z \frac{0.00844 \times 2.22}{s(s+2.22)} . \tag{32c}$$

This must be made equal to KG in equation 31, or the filter and preamplifier may be defined as

$$K_{\theta_x} F(s)_x = 127,000 \times \frac{0.2}{(s+0.2)} \times \frac{(s+2.35)}{2.35} \times \frac{(s+9.5)}{9.5} \times \frac{56.2}{(s+56.2)} \tag{33a}$$

$$K_{\theta_z} F(s)_z = 118,500 \times \frac{0.2}{(s+0.2)} \times \frac{(s+2.22)}{2.22} \times \frac{(s+9.5)}{9.5} \times \frac{56.2}{(s+56.2)} . \tag{33b}$$

5. Performance Check

The open loop transfer function of the overall system is defined as

$$\frac{\theta(s)}{e_\theta(s)} = \frac{1180(s+9.5)}{s(s+0.2)(s+56.2)} . \tag{34}$$

The relative stability of the servo loop is indicated by the Bode plots in Figure 30. It may be seen that adequate phase and gain margins exist.

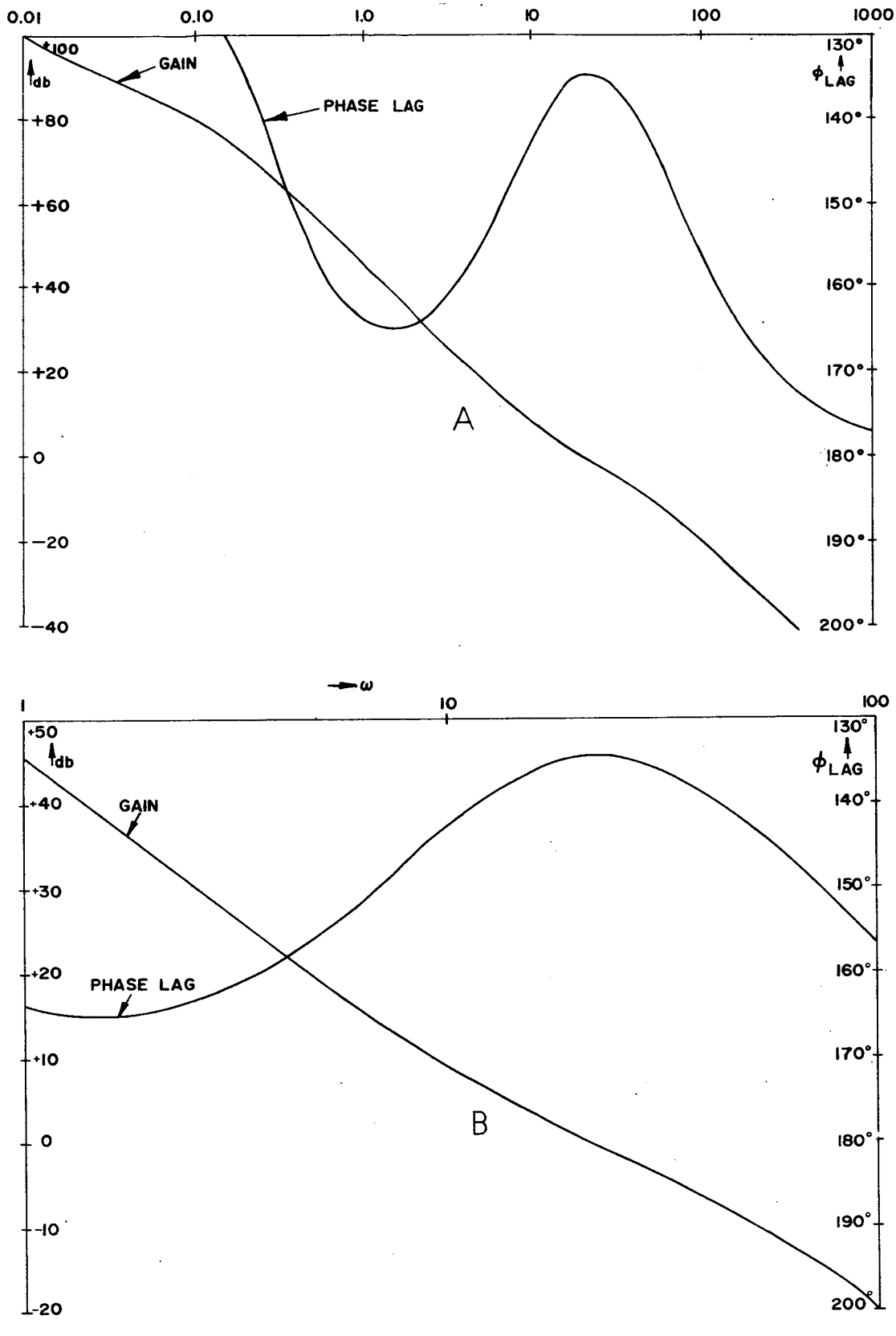

Figure 30. Open Loop Response.

The closed loop transfer function of the position loop is defined as

$$\frac{\theta(s)}{\overset{*}{\theta}(s)} = \frac{1180\,(s + 9.5)}{(s^2 + 28.3s + 400)\,(s + 28.1)} \tag{35}$$

This yields a response with a damping ratio of 0.7 and a natural frequency of 20 rad/s.

The frequency response of the closed loop tracking system is plotted in Figure 31.

The position error versus the command transfer function is

$$\frac{e_\theta(s)}{\overset{*}{\theta}(s)} = \frac{s\,(s + 0.2)\,(s + 56.2)}{(s^2 + 28.1s + 400)\,(s + 28.1)} \tag{36}$$

For a command ramp input, $\overset{*}{\theta}(s) = \frac{\overset{*}{\dot{\theta}}_o}{s}$, the steady-state position error is

$$e\,(0) = \frac{(0.2)\,(56.2)}{(400)\,(28.1)}\,\overset{*}{\dot{\theta}}_o = \frac{\overset{*}{\dot{\theta}}_o}{1000}. \tag{37}$$

This yields a maximum error for $\overset{*}{\dot{\theta}}_o = 5$ deg/s,

$$e_\theta\,(0) = 0.005 \text{ deg} = 18 \text{ arc sec} \tag{38}$$

which is below the maximum permitted tracking error of 20 arc sec.

The friction torque about the elevation axis that can be overcome by a static error of 5 arc sec is

$$T_{s_x} = e_{\theta_s} K_\theta K_{\dot{\theta}} \frac{K_t}{R} = 24 \times 10^{-8} \times 127{,}000 \times 2.25 \times 0.136 =$$

$$.932 \text{ mN.} \tag{39}$$

Thus a static position error of 5 arc sec about the elevation axis will saturate the torque motor if its maximum rating is less than .932 mN.

Similarly, the torque generated about the azimuth axis for a static error of 5 arc sec will be

$$T_{s_z} = e_\theta K_\theta K_\phi \frac{K_t}{R} = 24 \times 10^{-6} \times 118,500 \times 22.5 \times 0.136 =$$

$$8.70 \text{ mN.} \qquad (40)$$

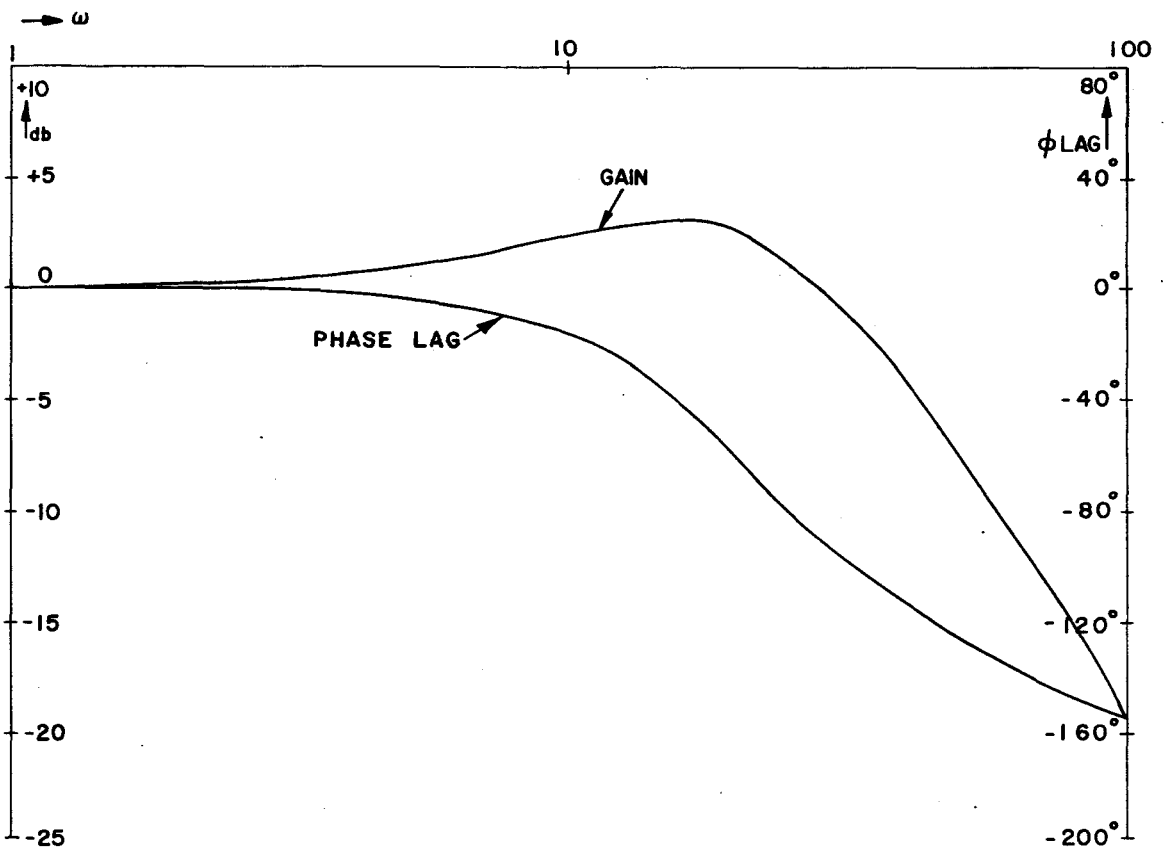

Figure 31. Closed Loop Response.

This means that the azimuth torquer will be saturated by a static position error of 5 arc sec if it cannot generate 8.70 mN.

The above torquers may be sized to overcome the breakaway friction of the system since the drive appears adequate to overcome any resistance it is likely to encounter.

E. CONCLUSIONS

In conclusion, it may be stated that a practical servo loop can be provided which will satisfy the requirements in the specifications. The design is preliminary and might require modification when detector noise or other data become available.

REFERENCES

1. Final Report - Study and Experimental Program Opdar Trajectory Measurement System. Engineering Report No. 7534, Perkin-Elmer Corporation, January 24, 1964.

2. Quarterly Reports, Contract NAS8-2661, Optical Guidance Feasibility Study, Data Corporation, Dayton, Ohio.

3. Introduction to Radar Systems, Merrill I. Skolvik, McGraw Hill Book Co., Inc., 1962, New York.

4. Regenerative Circulatory Multiple-Beam, Interferometry for the Study of Light Propagation Effects, Journal of the Optical Society of America, Vol. 52, No. 10, October 1962.

5. "General Radar Equation," W. M. Hall, Research and Development Handbook, Space Aeronautics, pp. D-11 to D-21, Vol. 38, No. 2, 1962-63.

6. Principles of Optics, Max Born and Emil Wolf, pp. 394-397, The MacMillan Company, New York, 1959.

7. Elements of Infrared Technology, P. W. Kruse, L. D. McGlauchlin, and R. B. McQuistion, John Wiley and Sons, Inc., New York, 1962.

8. Fundamentals of Optics, Jenkins and White, McGraw-Hill Book Co., Inc., New York, 1957.

9. Fundamental of Infrared Technology, Holter, Nudelman, Suits, Wolfe, and Zissis, The MacMillan Company, New York, 1962.

10. Encyclopedic Dictionary of Physics, Edited by J. Thewlis, Vol. 6, pp. 519-520, The MacMillan Company, New York, 1962.

11. "Model of the Atmospheric Radio Refractive Index," B. R. Bean and G. D. Thayer, Proceedings of the I.R.E., May 1959.

12. "A Study of Radar Elevation-Angle Errors Due to Atmospheric Refraction," B. M. Fannin and K. H. Jehn, I.R.E. Transactions on Antennas and Propagation, January 1957.

13. Study Phase Report for Precision Infrared Tracking System, Perkin-Elmer Report 7211, Oct. 13, 1962

BIBLIOGRAPHY

1. Study and Experimental Program (OPDAR) Trajectory Measurement System, Perkin-Elmer Corp., Jan. 24, 1964.

2. Electro-Optical Attitude Measuring System, Radio Corporation of America, Oct. 1963.

3. Textbook on Spherical Astronomy, W. M. Smart, Cambridge University Press, 1960.

4. "Radio Refraction in a Cool Exponential Atmosphere," J. R. Bauer, W. C. Mason, and T. A. Wilson, Lincoln Laboratory, R. R. 186, Aug. 27, 1958.

5. Principles of Optics, M. Born and E. Wolf, The MacMillian Company, 1959, New York.

6. "Effect of Atmospheric Horizontal Inhomogeneity," B. R. Bean and B. A. Cahoon, N. B. S., Vol. 63D, Nov. 1959.

7. Atmospheric Turbulence and Its Effect on Laser Communication Systems, Tech. Memorandum 69, North American Aviation, Oct. 18, 1963.

8. "Propagation at Great Heights in the Atmosphere," G. Millington, Marconi Review, Vol. 21, 1958.

9. "An Atmospheric Model," T. E. Sterne, The Astronomical Journal, March 1958.

10. A Manual of Spherical and Practical Astronomy, Vol. 1, William Chauvenet, Dover Publications, New York, 1960.

11. The A. R. D. C. Model Atmosphere 1956, R. A. Minzner and W. S. Ripley, AFCRC-TN-56-204.

12. An Attempt to Establish a Standard Atmospheric Density Profile Under Considerations of Its Time and Space Variations, RR-TR-3-60, Army Ballistic Missile Agency, Redstone Arsenal, Alabama, Dec. 30, 1960.

PRECISION OPTICAL TRACKING SYSTEM FOR ADVANCED LAUNCH VEHICLES

By Charles L. Wyman, Klaus Juergensen, Robert L. Kurtz,
Larry Hayes, and John M. Gould

The information in this report has been reviewed for security classification. Review of any information concerning Department of Defense or Atomic Energy Commission programs has been made by the MSFC Security Classification Officer. This report, in its entirety, has been determined to be unclassified.

This document has also been reviewed and approved for technical accuracy.

E. J. REINBOLT
Chief, Applied Physics Section

J. C. TAYLOR
Chief, Applied Research Branch

W. HAEUSSERMANN
Director, Astrionics Laboratory

DISTRIBUTION

R-DIR
Mr. Weidner

R-RP
Dr. Stuhlinger
Dr. Dozier
Dr. Mechtly

R-AERO
Dr. Geissler
Dr. Speer
Mr. Fulmer
Mr. Ladner
Mrs. McNair
Mr. Garcia
Mr. Emanuel

R-ASTR
Dr. Haeussermann
Mr. Richard
Mr. Weber
Mr. Digesu
Mr. Moore
Mr. Mandel
Mr. Hoberg
Mr. Fichtner
Mr. Hosenthien
Mr. Boehm
Mr. Angele
Mr. Taylor
Mr. Reinbolt
Mr. Hovik
Mr. Juergensen
Mr. Wyman (10)
Mr. Gould
Mr. Hayes
Mr. Kurtz
Dr. Randall
Mr. Evans
Miss Flowers
Reference File

MS-IP

MS-IPL (8)

MS-H

CC-P

Mr. Roland Chase (2)
OART, Code RET
Federal Office Bldg. 10B, Rm. 600
Washington 25, D. C.

Mr. John Walker
OART, Code RET
Federal Office Bldg. 10B, Rm. 600
Washington 25, D. C.

Scientific and Technical Information
Facility (25)
Attn: NASA Representative (S-AK/RKT)
P. O. Box 5700
Bethesda, Maryland

Mr. Henry Mancini/EMASI
Rome Air Development Center
Griffiss Air Force Base
Rome, Georgia

Mr. William Oneby
Electronic Service Division (ESD)
Hanscom Field
Bedford, Massachusetts